



Research Paper

Determination of layer charge density in expandable phyllosilicates with alkylammonium ions: A combined experimental and theoretical assessment of the method

Bruno Lanson^{a,*}, Pierre Mignon^b, Mélusine Velde^{a,c,d}, Andreas Bauer^c, Martine Lanson^a, Nathaniel Findling^a, Carlos Perez del Valle^e

^a Univ. Grenoble Alpes, Univ. Savoie Mont Blanc, CNRS, IRD, Univ. Gustave Eiffel, ISTerre, F-38000 Grenoble, France

^b Univ. Lyon, Univ. Claude Bernard Lyon 1, CNRS, Institut Lumière Matière, F-69622 Villeurbanne, France

^c Friedrich-Schiller-University Jena (FSU), Institute of Geosciences, Applied Geology, Burgweg 11, 07749 Jena, Germany

^d University of Chicago, Department of Biological Sciences, Chicago, USA

^e Univ. Grenoble Alpes, CNRS, DCM, F-38000 Grenoble, France



ARTICLE INFO

Keywords:

Layer charge

Expandable phyllosilicates

Alkyl ammonium method

X-ray diffraction

Simulation

ABSTRACT

Layer charge deficit is a key crystal-chemical parameter for the classification and nomenclature of 2:1 phyllosilicates that also controls some of their fundamental properties such as cation exchange capacity, expandability, water content, or rheology. The clay community has thus devoted significant efforts to determine this parameter either from the smectite/vermiculite chemical composition (the structural formula method) or experimentally using the alkylammonium method, that theoretically allows the determination of the mean layer charge density and of its distribution. In the present study density functional theory (DFT) and molecular dynamics (MD) simulations are compared to experimental X-ray diffraction data for a series of synthetic saponites with layer charge ranging from medium-charge smectite to medium-charge vermiculite. Consistency of computed and measured layer-to-layer distances confirms the ability of computational approaches to accurately predict the organization of alkylammonium cations in smectite interlayers. Thermalization of DFT-optimized structure models through MD simulations allows probing possible alternative interlayer configurations such as the electrostatically-favored location of ammonium heads above/below Al-substituted tetrahedra. X-ray diffraction results showed that layer-to-layer distances intermediate between those corresponding to the stable h1, h2, etc. interlayer configurations described in the literature result from the interstratification of different stable configurations. The overall consistency of computational and experimental results confirms also the ability of the alkylammonium method to accurately determine a mean value of layer charge density consistent with smectite structural formula when using the revised equations proposed by Laird et al. (1989). The validity of the method appears however limited to smectite-group minerals [layer charge density ranging from ~ 0.5 to ≤ 1.2 per $O_{20}(OH)_4$] most likely owing to the coexistence of both stable “layered” and paraffin-like interlayer configurations for higher values of layer charge. In addition, this consistency challenges the ability of the method to quantitatively describe distributions of layer charge in expandable phyllosilicates even when using the complete series of alkylammonium cations.

1. Introduction

Classification and nomenclature of 2:1 phyllosilicates rely to a large extent on their layer charge deficit (Guggenheim et al., 2006). This key crystal-chemical parameter allows indeed differentiating talc-phyllite, smectite, vermiculite, interlayer-deficient mica, true

mica, and brittle mica groups of 2:1 phyllosilicates (Guggenheim et al., 2006). Furthermore, layer charge controls fundamental properties of the phyllosilicates such as cation exchange capacity (Jackson, 2005; Dohrmann, 2006 and references therein), expandability (Laird, 2006), or water content (Sato et al., 1992; Ferrage et al., 2007). Similarly, layer charge density controls to a large extent clay swelling through the

* Corresponding author.

E-mail address: bruno.lanson@univ-grenoble-alpes.fr (B. Lanson).

<https://doi.org/10.1016/j.clay.2022.106665>

Received 15 April 2022; Received in revised form 3 August 2022; Accepted 7 August 2022

0169-1317/© 2022 Elsevier B.V. All rights reserved.

hydration of interlayer cations (Ferrage et al., 2011; Dazas et al., 2015; Vinci et al., 2020), and is thus an essential parameter for the design of engineered clay barriers, including their self-healing ability (Gates et al., 2009), and rheological properties of clay suspensions (Christidis et al., 2006; Paineau et al., 2011a, 2011b). Abundance and nature of expandable 2:1 layer silicates (smectite and vermiculite groups) also have, together with organic matter, a key influence on soil fertility.

The pivotal influence of layer charge density on properties of expandable phyllosilicates has induced significant efforts from the clay community to determine theoretically this crystal-chemical parameter from the smectite/vermiculite chemical composition (the so-called structural formula method, SFM – Newman and Brown, 1987; Cical and Komadel, 1994; Laird, 1994) or experimentally. In this context, the so-called alkylammonium method (AAM) initially developed by Lagaly, Weiss, and co-workers (Lagaly and Weiss, 1969, 1971; Lagaly, 1994) appears especially well suited, allowing the determination of the mean layer charge density and of its distribution. The method relies on the experimental determination of unit-cell d_{001} parameter for phyllosilicates intercalated with alkylammonium cations of increasing chain lengths (Lagaly, 1994). As the original method is time consuming for routine analysis, simplified methods have been proposed (Olis et al., 1990; Dohrmann et al., 1999). These methods commonly use a limited number of alkyl chain lengths to determine the mean layer charge density. Considerable efforts have also been devoted to reconcile the results obtained from SFM and AAM (Laird, 1994; Kaufhold, 2006; Kaufhold et al., 2011).

In parallel to the experimental AAM, molecular dynamics (MD) has been used to provide insights into the molecular-level interactions responsible for the experimentally observed changes in layer-to-layer distances as a function of alkyl chain length (Heinz et al., 2007; Liu et al., 2007). In these studies, computational results were assessed against experimental literature data obtained on natural smectites whose layer charges scatter essentially over the whole range allowed for smectite (Lagaly and Weiss, 1971; Laird et al., 1989; Vaia et al., 1994). Comparison of MD simulations computed properties with data supported the robustness of the modelling approach and its ability to describe the organization of large organic molecules in smectite interlayers although some specific aspects remained unclear. The first issue is related to the underestimation of layer charge densities derived from the strict application of the AAM compared to those resulting from the SFM, this AAM known bias challenging the consistency between computed and experimental results. A second issue is related to smectite interlayer structure in transition zones between the well-defined configurations described by Lagaly and coworkers (Lagaly and Weiss, 1969, 1971; Lagaly, 1994). In the method description (Lagaly, 1994), layer-to-layer distances intermediate between those of the well-defined configurations correspond to their coexistence/interstratification whereas they correspond to a unique “stable” configuration in the simulations (Heinz et al., 2007; Liu et al., 2007).

The present study aims at investigating these two specific aspects. For this purpose the AAM was used on four synthetic samples whose layer charge densities range from medium-charge smectite to medium-charge vermiculite [0.8 to 1.4 per $O_{20}(OH)_4$]. The use of synthetic samples aimed at minimizing the heterogeneity of layer charge density for a given sample and at improving crystallinity to minimize experimental bias related to peak broadening (Stanjek and Friedrich, 1986; Stanjek et al., 1992; Mermut, 1994). Simulations were performed with both density functional theory (DFT) to determine interlayer configurations most symmetrical and most stable at 0 K and MD approaches that allow calculation of more realistic configurations after thermalization at 300 K.

2. Materials and methods

2.1. Smectite synthesis

A set of expandable phyllosilicates with a common structural formula $^{inter}[Na_x]^{oct}[Mg_6]^{tet}[Si_{8.0-x}Al_x]O_{20}(OH)_4$ and a layer charge (x) varying from 0.8 to 1.4 per $O_{20}(OH)_4$ were synthesized hydrothermally from gel precursors in an externally heated Morey-type pressure vessel with an internal silver tubing (Hamilton and Henderson, 1968; Robert et al., 1993; Bergaoui et al., 1995), as described previously (Dazas et al., 2015). A temperature of 400 °C, a water pressure of 1 kbar, and a duration of 4 weeks were used for synthesis. After synthesis, all samples were Na-saturated at room temperature by contact with 1 mol·L⁻¹ aqueous solutions of NaCl. Excess NaCl was removed by rinsing the solid by immersion for 24 h in deionized water (Siemens UltraClear, 18.2 MΩ·cm) and separation of the solid fraction by centrifugation. Resulting monomineralic synthetic saponites are hereafter referred to as Sap-OH-x. Previous studies of samples prepared using the same experimental protocols for gel preparation and synthesis supported, from nuclear magnetic resonance and Ar adsorption data, an homogeneous distribution of Al substitutions in saponites, whatever the layer charge (Sanz and Robert, 1992; Michot and Villieras, 2002; Sanz et al., 2006).

2.2. Alkylammonium method

2.2.1. Preparation of alkyl chains

Homoionic saturation of saponites with alkylammonium cations having different carbon chain lengths required the preparation of solutions with these cations from alkylamines of proper chain length (Table S1). Preparation of alkylammonium cation solutions was described by Lagaly (1994). In brief, the required amount of alkylamine (Table S2) was weighed and stirred and dissolved in 100 mL of ethanol in a 1000 mL beaker. Next, 400 mL of ultrapure water were added to the solution while maintaining the stirring, commonly leading to the formation of a precipitate. Suspension was then titrated with hydrochloric acid to pH 7.0. Concentrations and approximate volumes of hydrochloric acid solutions required for the titration are reported in Table S2. For short chain lengths, heat production during titration of the solutions required controlling temperature with a water bath. For chain lengths ranging 14–18 carbons, the precipitate did not disappear when acid was added; ethanol (approximate volumes listed in Table S2) was then added to the stirred suspension to allow for a complete dissolution of the precipitate. If necessary, precipitate dissolution was enhanced by heating the suspension to ~50 °C using a water bath. When clear and pH neutral solutions were obtained, ultrapure water was added to a final volume of 1000 mL of appropriate alkylammonium cation concentrations (Table S2).

2.2.2. Smectite saturation with alkylammonium cations

Homoionic saturation of saponites with alkylammonium cations having different carbon chain lengths was performed in 10 mL Teflon tubes using ~100 mg of synthetic saponite. After addition of 2 mL of the appropriate alkylammonium solution (4 mL for chains longer than 13C atoms), the suspension was shaken vigorously. Tubes were shaken until foam, that may contain clay particles, disappeared. Tubes were then heated to 65 °C in an oven for 24 h, tube caps remaining slightly open. The cation-exchanged smectites were then centrifuged and rinsed with ethanol (2 mL per rinsing step). Rinsing steps were repeated 8–10 times until the ethanol supernatant did not leave white traces when dried on a glass slide. Alkylammonium-exchanged smectites were then finally air dried at room temperature overnight.

2.3. XRD data collection and processing (alkylammonium method)

For all samples, oriented slides were prepared by drying at room temperature a clay suspension in ethanol on glass slides. XRD patterns

were then recorded using a Bruker D8 diffractometer equipped with a MHG Messtechnik humidity controller coupled to an Anton Paar CHC+ chamber. Intensities were measured with a SolXE Si(Li) solid-state detector (Baltic Scientific Instruments) for 4 s per 0.04° 2θ step over the $2\text{--}50^\circ$ 2θ Cu K α angular range. Divergence slit, the two Soller slits, the antiscatter, and resolution slits were 0.3° , 2.3° , 0.3° , and 0.1° , respectively. Samples were kept at 23°C in the CHC+ chamber during the whole data collection. Samples were kept also under a constant flow of mixed dry/saturated air to maintain a 5% relative humidity (RH) to minimize hydration of smectite interlayers. RH was continuously monitored with a hygrometer (uncertainty of $\sim 2\%$ RH) located close to the sample.

The alkylammonium method was performed assuming a systematic surface area of the unit cell of 49 \AA^2 within the **ab** plane and no correction for particle size [$A_c = 5.67 \times N_c + 14$; $\sigma' = 49 / (2 \times A_c)$] in which A_c is the average planar area associated with each alkylammonium cation of carbon chain length N_c , σ' being the layer charge corresponding to the critical carbon chain length causing the transition from h1 to h2 configurations – (Lagaly, 1981)]. The revised equation ($\sigma'' = 1.672 \times \sigma' - 0.156$) proposed by Laird et al. (1989) was preferred however to ease the comparison with layer charge density determined from the structural formula, that is in the present case with layer charge density determined from the stoichiometry of the synthetic products. In addition, the use of synthetic smectites with an enhanced homogeneity and extent of coherent layer stacking along the c^* axis allowed minimizing reflection broadening and no correction of peak position was performed (Stanjek and Friedrich, 1986; Stanjek et al., 1992; Mermut, 1994).

2.4. Density functional theory (DFT) simulations

Crystal models defined with general structural formula $\text{Mg}_6\text{Si}_{8.0-x}\text{Al}_x\text{O}_{20}(\text{OH})_4.\text{NH}_3(\text{CH}_2)_n\text{CH}_3$, $x = 1.0$ and 1.5 , and $n = 1, 2$, etc. were used for DFT simulations. Simulations were performed using a $2a \times 1b \times 1c$ super-cell for $x = 1.0$, and a $2a \times 2b \times 1c$ super-cell for $x = 1.5$. Interlayer displacement was allowed to vary during the simulations. Within these super-cells, distributions of Al-substituted tetrahedra and of interlayer alkylammonium cations were generated to obey Löwenstein rule (no adjacent Al-substituted tetrahedra) and to be as regular as possible, consistent with the homogeneous distribution of Al substitutions in saponites reported in the literature (Sanz and Robert, 1992; Michot and Villieras, 2002; Sanz et al., 2006). Periodic DFT calculations were performed with the Siesta 4.0b-485 code (Soler et al., 2002) using a generalized gradient approximation and a Perdew-Burke-Emzerhof correlation-exchange functional with a mesh cut-off of 500Ry and 6 and 9 k-points in the Monkhorst Pack grid (Hernández-Haro et al., 2016). Troullier-Martins norm-conserving pseudopotentials (Troullier and Martins, 1991) and numerical atomic orbital and double ξ plus polarization basis sets were also used for calculations. DFT methods are well suited to described systems containing cations as interlayer species as the present ones (Hernández-Haro et al., 2016).

2.5. Molecular dynamics (MD) simulations

Classical MD simulations were performed for saponites having layer charges similar to those of the synthetic products: $x = 0.8, 1.0, 1.2$, and 1.4 per $\text{O}_{20}(\text{OH})_4$. Initial atomic positions for both the clay layer and interlayer were derived by replicating the DFT optimized configurations in a $6a \times 4b \times 1c$ super-cell, and using the DFT-optimized layer displacement. For $x = 0.8$ and $x = 1.0$, initial positions were obtained from DFT configurations optimized for $x = 1.0$; and for $x = 1.2$ and $x = 1.4$, DFT configurations optimized for $x = 1.5$ were used. Owing to the replication of DFT optimized cells, substitutions are regularly distributed in the super-cells used for MD simulations. When necessary, layer charge was decreased by switching Al-substituted tetrahedral sites back to Si occupancy and removing the associated alkyl molecule (total

number of substitutions in Table S3). Charge adjustments were performed to maintain the distribution of Al-substituted tetrahedra as regular as possible.

MD simulations were performed using ClayFF force field for the clay model (Cygan et al., 2004) whereas alkylammonium parameters were obtained from DFT calculations at the B3LYP/6-31G* level performed with the Gaussian software. Alkylammonium molecules were optimized in the gas phase and RESP (restrained electrostatic potential) partial atomic charges, that allow reproducing the electrostatic potential of molecular boundaries, were used as molecular net charges in the force-field simulations (Woods and Chappelle, 2000). The general Amber force field (Wang et al., 2004), which is extensively used for organic molecules modelling and reproduces well their structure and dynamics (Hobza et al., 1997; Young et al., 1997; Thyveetil et al., 2008; Swadling et al., 2013; Szczerba et al., 2014; Szczerba and Kalinichev, 2016; Corbin et al., 2021), was used to generate alkylammonium molecular parameters. Lorentz-Berthelot rules were applied for Lennard-Jones inter force fields parameters. Amber and ClayFF force fields are rather simple to combine as they both use harmonic potential for bond terms, although ClayFF does not use angle and dihedral terms. This approach has already been successfully used in various theoretical studies (Thyveetil et al., 2008; Swadling et al., 2010, 2013; Mignon et al., 2020; Corbin et al., 2021). Periodic boundary conditions were applied in all three spatial directions.

The large-scale atomistic/molecular massively parallel simulator (LAMMPS – Plimpton, 1995) was used for all simulations, which were performed at 300 K and 1 atm. A 12 \AA cutoff was used for electrostatic and Lennard-Jones interactions. Coulombic interactions were computed by Ewald summation and the particle-particle-particle-mesh method at a 0.0001 accuracy. The equilibration procedure consisted first in warming up the system in the NVT ensemble. The system was then allowed to relax along all directions in the NPT ensemble to model the interlayer space in real conditions and density. The system was then equilibrated through a two-step procedure increasing time steps from 0.1 to 0.5 fs. The initial equilibration run included a total of 1,200,000 time steps. A second NPT simulation was then run for 600,000 time steps during which the average d_{001} was determined to be compared with experimental results. A final NVT simulation (600,000 time steps) was run to compute structural data. Octahedral Mg atoms were kept fixed during all simulations by imposing forces to be null. This allowed minimizing translations within the layer plane and induced systematic location of Mg atoms at the origin of the unit cell (Mignon et al., 2020; Corbin et al., 2021).

3. Results and discussion

3.1. X-ray diffraction

As expected for smectites hosting interlayer alkylammonium cations, positions of reflections present in the XRD patterns of Sap-OH-0.8 indicated an increase of the layer-to-layer distance (LLD) with increasing chain length (Figs. 1, 2). For Sap-OH-0.8, two “plateaus” corresponding to LLDs of ~ 13.4 and $\sim 17.6 \text{ \AA}$ were observed for $n = 3\text{--}9$, and $n = 16\text{--}18$, respectively. The two “plateaus” correspond to the LLDs of monolayers and bilayers of alkylammonium cations [defined as interlayer h1 and h2 configurations, respectively at 13.4 and 17.6 \AA by Lagaly, 1994], for which alkyl chains are essentially parallel to the layer surface. Between these two plateaus, the apparent basal distance increased steadily as described by Lagaly (1994). When increasing the charge density from $x = 0.8$ to $x = 1.0, 1.2$, and 1.4 , h1 and h2 configurations were observed for decreasing chain lengths (Figs. 2, 1, S1–S3), consistent with the basics of the method (Lagaly, 1994). A third plateau at $\sim 22 \text{ \AA}$, typical for the pseudotrimolecular layers of alkylammonium cations (h3 interlayer configuration – Lagaly, 1994) was observed for high-charge samples and long alkylammonium chains ($x = 1.2\text{--}1.4$ and $n = 16\text{--}18$ – Figs. 2, S2–S3).

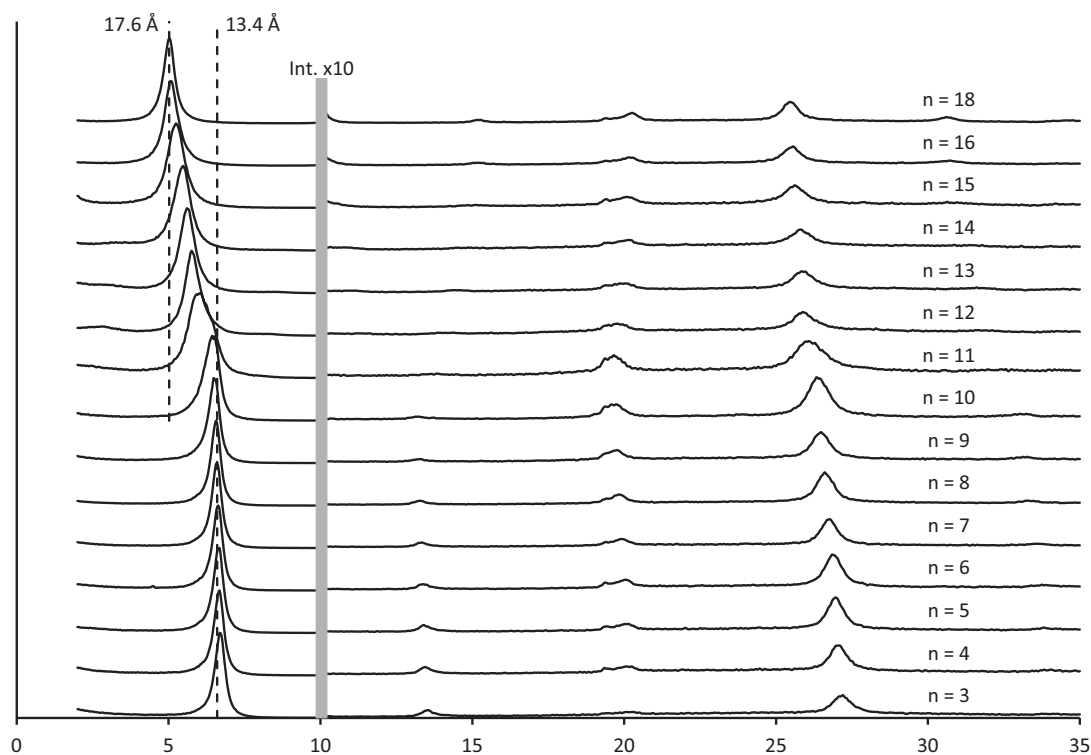


Fig. 1. X-ray diffraction patterns recorded on Sap-OH-08 as a function of the alkyl chain length of the interlayer alkylammonium cation (expressed as the number *n* of carbon atoms in the alkyl chain). Data were collected at 5 %RH. Dashed lines indicate the layer-to-layer distances typical for monolayers and bilayers of interlayer alkylammonium cations [h1 and h2 configurations of Lagaly, 1994, respectively].

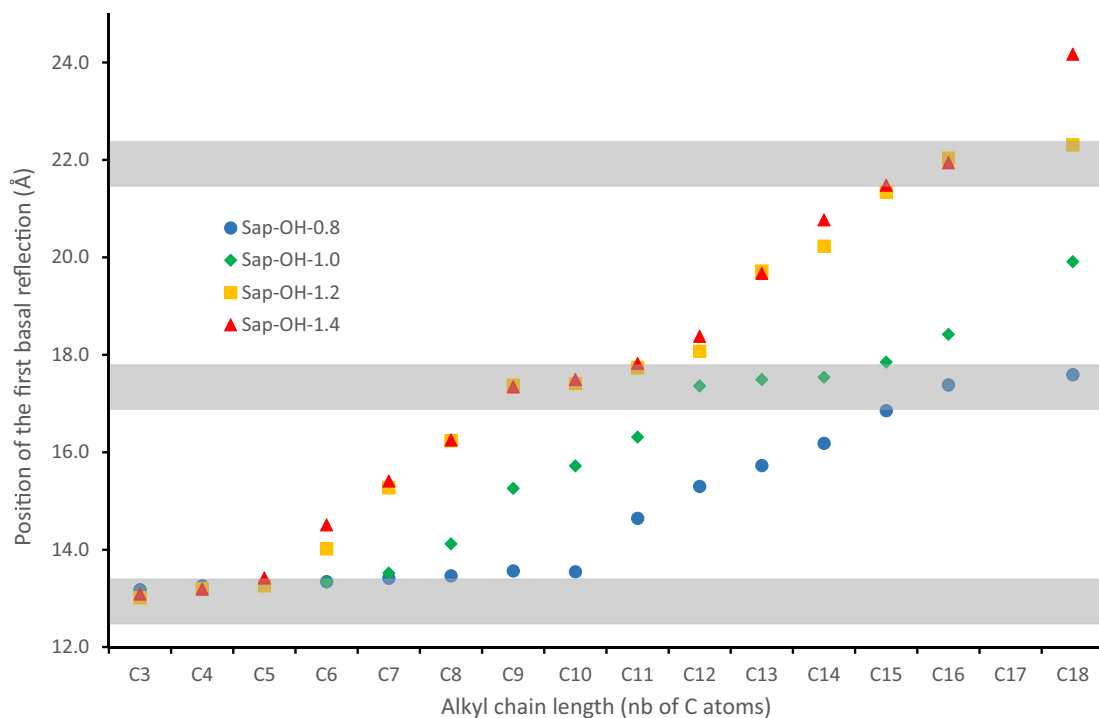


Fig. 2. Evolution of the position of the first experimental basal reflection as a function of the alkyl chain length. Greyed zones correspond to the layer-to-layer distances typical for monolayers, bilayers, and pseudotrimolecular layers of interlayer alkylammonium cations [h1, h2, and h3 configurations of Lagaly, 1994 at ~13.4, 17.6, and 22 Å, respectively].

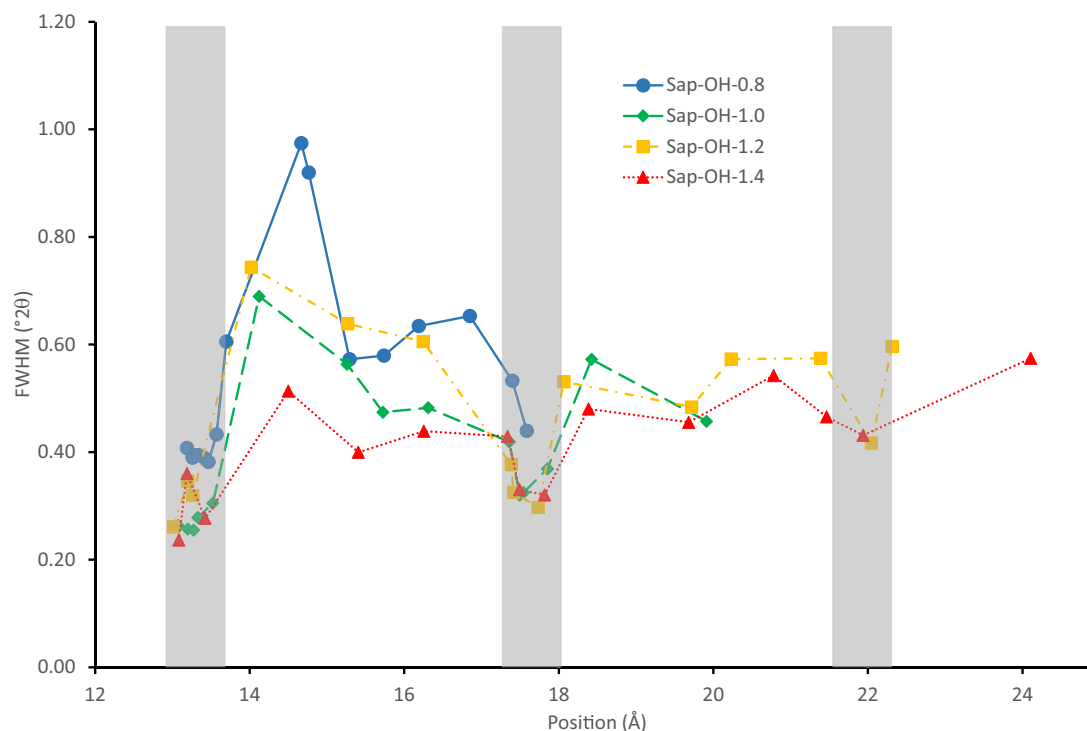


Fig. 3. Evolution of the full width at half maximum intensity (FWHM) of the first low-angle reflection as a function of its position. Greyed zones as in Fig. 2.

When plotting the full width at half-maximum intensity (FWHM) as a function of peak position, three local minima were visible (Fig. 3). Minimum FWHM values were observed for apparent LLDs corresponding to h1, h2, and h3 configurations. The significant increase in FWHM between these three minima results from the interstratification of different stable configurations within the same crystals (Méring, 1949; Moore and Reynolds Jr, 1997; Aristilde et al., 2013), consistent with the prediction of Lagaly (1994). Apparent LLDs intermediate between those of the stable configurations thus correspond to the coexistence within the same crystals (interstratification) of two stable configurations rather than to intermediate configurations as consistently observed for smectite hydration (Ferrage et al., 2005, 2010; Ferrage, 2016) and cation/anion exchange in clays and layer double hydroxides (Glaeser and Méring, 1954; Méring and Glaeser, 1954; Feng et al., 2006; Möller et al., 2010; Taviot-Guého et al., 2010; Lanson, 2011 and references therein).

Layer charge densities deduced from the evolution of XRD peak position with alkylammonium chain length increased consistently with the stoichiometry of the synthetic products. When using the original equation of Lagaly (1994), experimentally determined charge densities were 0.52, 0.69, 0.86, and 0.88 for Sap-OH- x with $x = 0.8, 1.0, 1.2,$ and 1.4 , respectively. As shown previously by Laird et al. (1989), values deduced from the original alkylammonium method (Lagaly, 1994) are systematically and significantly shifted towards lower values compared to those deduced from smectite stoichiometry and may be corrected to minimize this discrepancy. When using the revised equation proposed by Laird et al. (1989), layer charge densities determined using the modified alkylammonium method became 0.72, 0.99, 1.28, and 1.31 for Sap-OH- x with $x = 0.8, 1.0, 1.2,$ and 1.4 , respectively. Corrected values were significantly closer to those deduced from smectite stoichiometry, consistent with the conclusions of Laird et al. (1989). No significant difference was observed between Sap-OH-1.2 and Sap-OH-1.4, however, possibly indicating a limited sensitivity of the method for high layer charge densities.

3.2. DFT and MD simulations

In the present work, DFT simulations allowed determining interlayer configurations most stable at 0 K. These optimal configurations, highly symmetrical owing to the limited system size, were then used to derive initial inputs for MD simulations that allowed calculation of more realistic configurations after thermalization at 300 K. As a result, layer-to-layer distances computed from both DFT and MD simulations were essentially similar for a given layer charge and alkyl chain length (Fig. 4b,d), although thermal expansion was noticeable. Specifically, the two computational approaches used in the present study allowed describing the three stable configurations initially proposed by Lagaly (h1, h2, h3 – 1994), consistent with previous computational studies (Heinz et al., 2007; Liu et al., 2007).

3.2.1. Interlayer structure of the different stable configurations

Fig. 4 also shows that LLDs derived from both DFT and MD simulations were close to the values obtained experimentally for a given layer charge and alkyl chain length. Slightly larger LLDs were systematically obtained from MD simulations compared to DFT however. Unit-cell expansion most likely results from thermal motion which is implicit in MD simulations performed at 300 K, compared to the initial structures optimized at 0 K in DFT calculations. Computed LLDs were also consistent with those computed from classical MD simulations by Heinz et al. (2007), although systematically lower (by ~ 0.50 – 1.25 Å – Fig. 4a, c), possibly as the result of different charge location (tetrahedral substitutions in the present case) and of the induced contrasting under-saturation of surface O atoms. In addition, the starting model used in the present study for MD simulations was derived from DFT simulations optimized at 0 K and thus corresponding to minimal LLD. In their study Heinz et al. (2007) compared their results with LLDs from the literature that are systematically higher than those obtained experimentally in the present study. As a result, the apparent discrepancy between computed and experimental values was larger in the present study although calculated LLDs were lower, and closer to experimental LLDs obtained in the present work. This may be due to the improved crystallinity of the

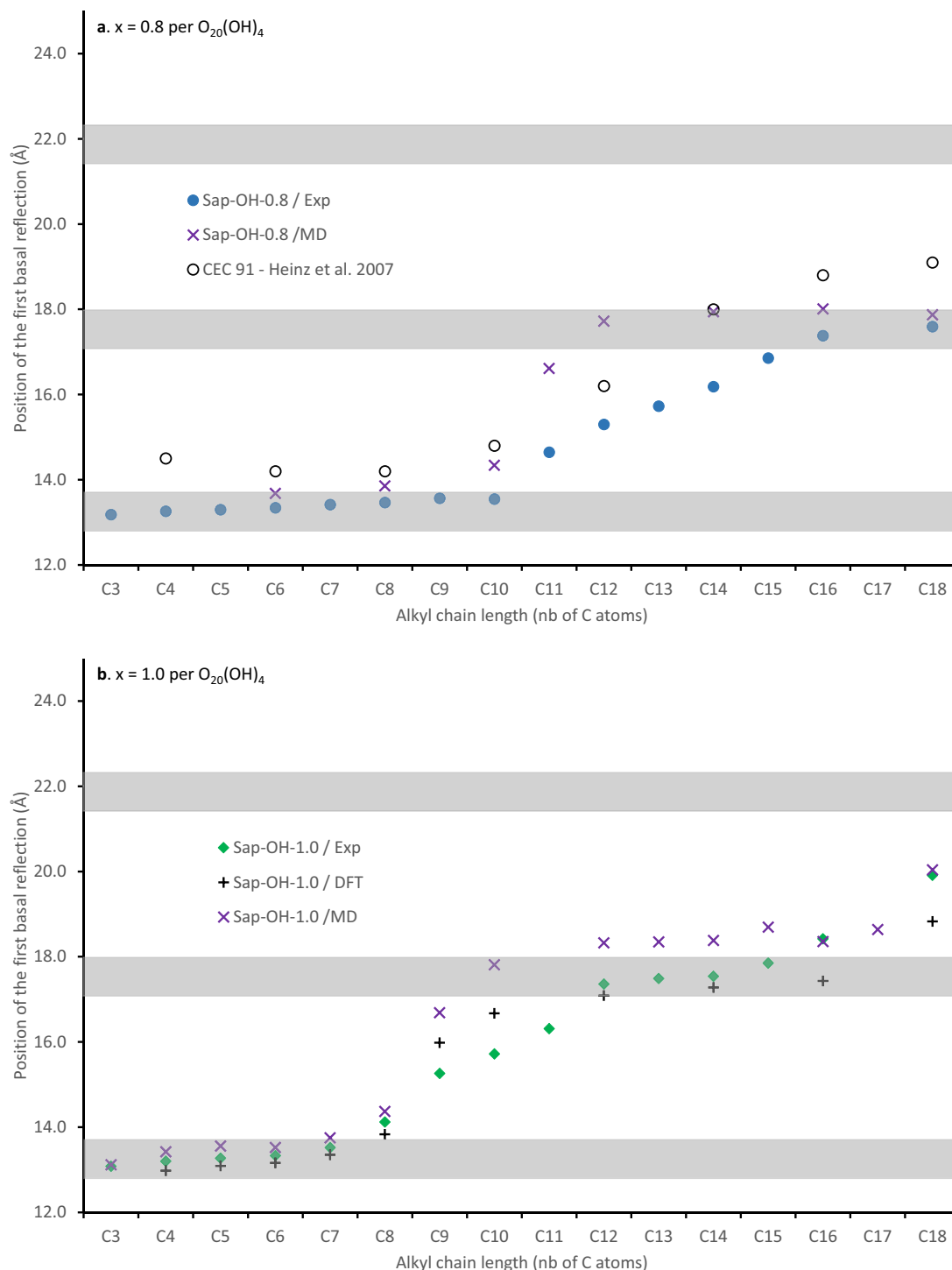


Fig. 4. Comparison of the layer-to-layer distance as a function of the alkyl chain length obtained experimentally (Fig. 2) with those derived from density functional theory (DFT) or molecular dynamics (MD) simulations. Patterns as in Fig. 2.

synthetic smectite used in the present study that allowed minimizing positional shifts of diffraction peaks related to size-broadening (Stanjek and Friedrich, 1986; Stanjek et al., 1992; Mermut, 1994).

Alkylammonium cations located in saponite interlayers were distributed with the ammonium heads pointing towards layer surfaces to compensate efficiently for the layer charge deficit through H-bonding (Figs. 5, 6, 7a, S4a, S5a). In DFT-optimized structures, ammonium NH_3^+ heads were located essentially above/below the ditrigonal cavity and

bound to the layer through $N-H \cdots O-H$ and $N-H \cdots O-(Si,Al)$ H-bonds (see inset in Fig. 5b). Location of $R-NH_3^+$ head groups above the ditrigonal cavity is consistent with results obtained by Heinz et al. (2007) and allows for a maximum compression of the system at 0 K.

DFT-computed $N-H \cdots O-(Si,Al)$ bond lengths between H atoms of the ammonium head and surface O atoms from $(Si,Al)O_4$ tetrahedra scattered from 1.7–1.8 Å correspond to the range observed for Al tetrahedra 1.85–1.95 Å correspond to the range observed for Si tetrahedra,

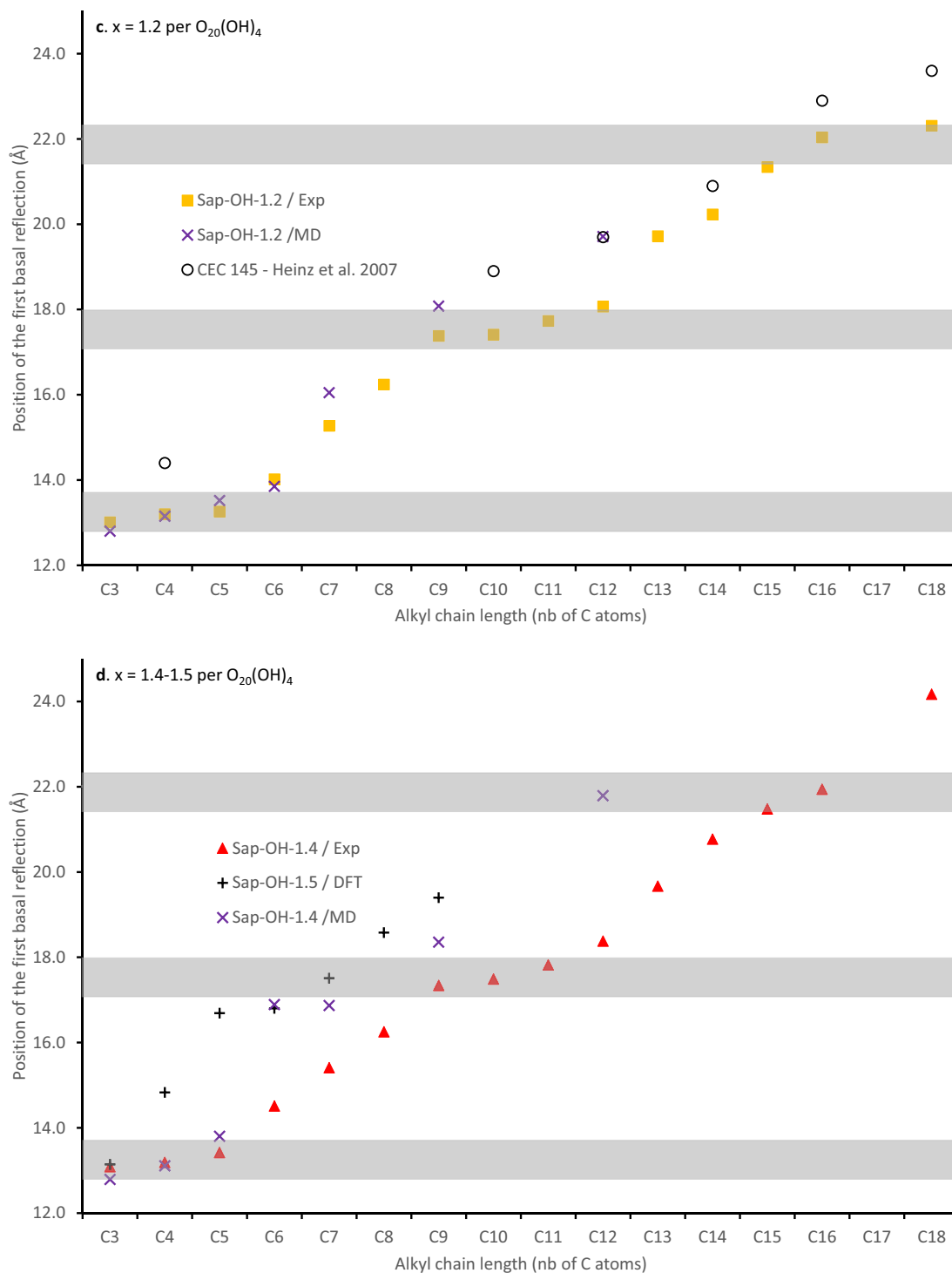


Fig. 4. (continued).

respectively. These distances were consistent with the long $N\bullet\bullet Al$ distances (3.45–3.55 Å) obtained from thermalized MD simulations (Fig. S6) but significantly larger than the 1.5 Å reported by Heinz et al. (2007) for $O\bullet\bullet H$ distances, despite the shorter LLDs obtained in the present study, consistent with XRD data. In the model used by Heinz et al. (2007), only octahedral substitutions were considered and electrostatic forces may be over-estimated. Indeed, ammonium head charges were adjusted arbitrarily to $+0.7 e^-$ charge per ammonium head for all alkyl chains whereas parameters DFT computed RESP charges obtained in the present study indicated lower positive charges. Despite the

induced longer H-bonds observed in our models compared to those reported by Heinz et al. (2007), shorter LLDs were obtained for stable h1 and h2 domains, consistent with experimental LLDs (Fig. 4). In addition to the position above/below the ditrigonal cavity, MD simulations performed in the present study indicated that in thermalized systems ammonium heads may also be located above/below Al-substituted tetrahedra leading to shorter $N\bullet\bullet O(Si,Al)$ distances (2.85–2.95 Å – Fig. S6), consistent with previous reports (Chen et al., 2017). This alternative configuration allows for an improved local charge compensation of undersaturated surface O atoms from Al-substituted tetrahedra

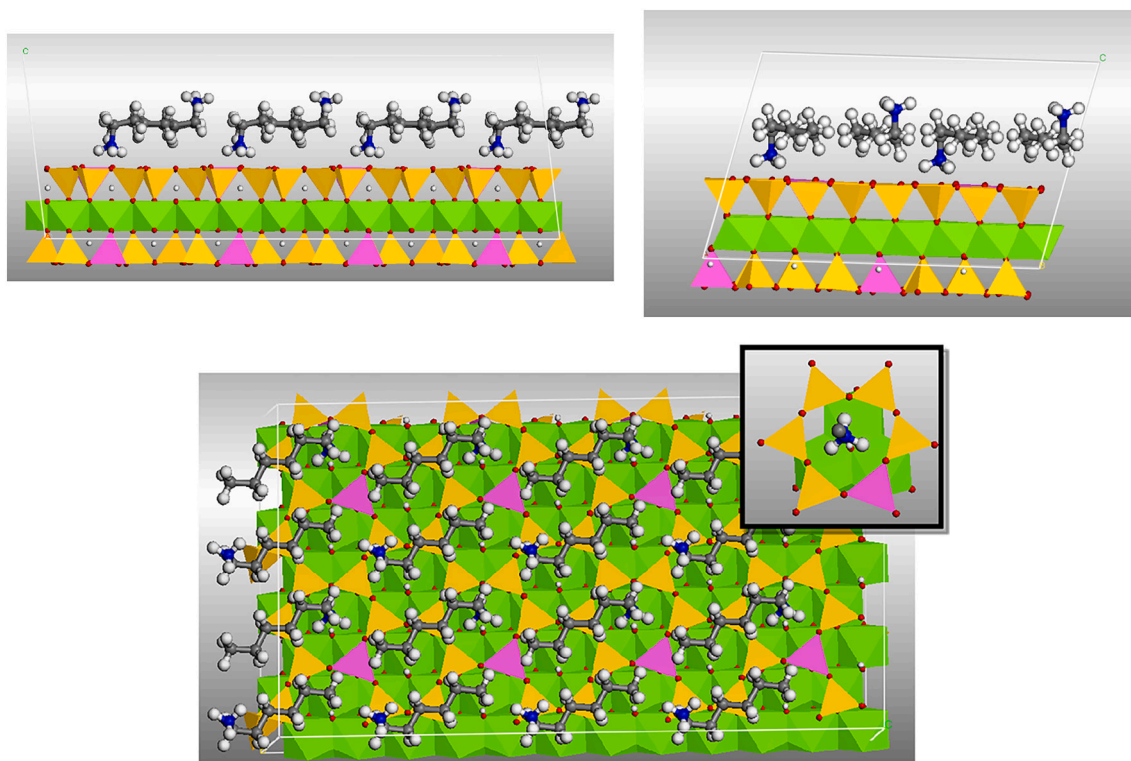


Fig. 5. DFT optimized configuration of saponite interlayer hosting a monolayer of alkylammonium cations [interlayer h1 configuration – Lagaly, 1994]. Layer charge: $x = 1.0$, alkyl chain length of the interlayer alkylammonium cation: 6 carbons. (a) Left and right, views along a and b axes, respectively. Si, Al, and Mg polyhedra are shown in orange, magenta, and green, respectively. O, N, C, and H atoms are shown as red, blue, and dark and light grey balls, respectively. Snapshots generated using Materials studio. (b) View along the c^* axis. Inset: Close-up on N-H...O-(Si,Al) bonding. Colors as in Fig. 5. Snapshots generated using Materials studio. (For interpretation of the references to colour in this figure legend, the reader is referred to the web version of this article.)

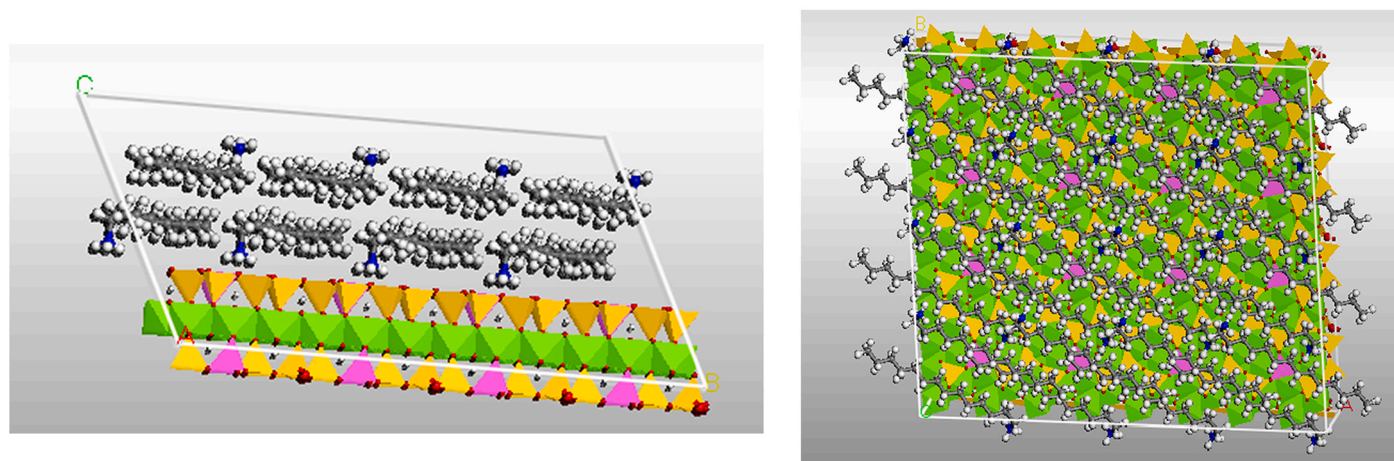


Fig. 6. DFT optimized configuration of saponite interlayer hosting a bilayer of alkylammonium cations [interlayer h2 configuration – Lagaly, 1994]. Layer charge: $x = 1.0$, alkyl chain length of the interlayer alkylammonium cation: 14 carbons. (a) From top to bottom, view along the a axis. Colors as in Fig. 5. Snapshots generated using Materials studio. (b) View along the c^* axis. Colors as in Fig. 5. Snapshots generated using Materials studio.

and for an improved electrostatic stabilization but results in slightly larger LLD values, as computed for thermalized systems. From the present MD simulations, this configuration appeared to be favored for saponites having the lowest charge ($x = 0.8$ – data not shown) owing to the presence of localized tetrahedral charges and to minimum steric constraints. Increasing layer charge density results in a layer charge distribution that is more homogeneous and in the sole location of ammonium heads above/below ditrigonal cavities thus allowing a stronger steric compression in the interlayers of higher charge saponites.

Although no specific simulations were performed, location of ammonium heads above/below the ditrigonal cavity is thus most likely favored by the presence of multiple Al-substituted tetrahedra among those defining this cavity. As a consequence, such a distribution of Al-substituted tetrahedra that could result, for example, from a non-homogeneous distribution of isomorphic Al-for-Si substitutions does not appear to challenge the validity of the alkylammonium method which relies primarily on steric constraints. Consistently, the alternative configuration of ammonium heads above/below Al-substituted

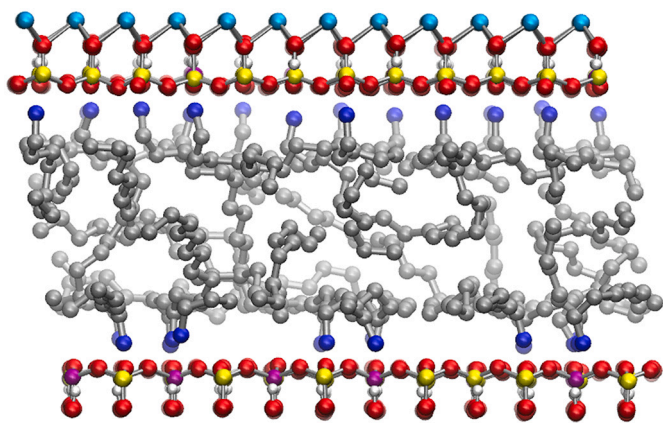


Fig. 7. Representative MD snapshots of saponite interlayer hosting a pseudotrilayer of interlayer alkylammonium cations. Layer charge: $x = 1.4$, alkyl chain length of the interlayer alkylammonium cation: 12 carbons. View along the b axis. Si, Al, Mg, O, N, C, and H atoms are shown as yellow, magenta, light blue, dark blue, dark grey, and white balls, respectively. H atoms from the alkylammonium cations are not shown. (For interpretation of the references to colour in this figure legend, the reader is referred to the web version of this article.)

tetrahedra was absent from the simulations performed by Heinz et al. (2007) whatever the layer charge considered, most likely as the result of the octahedral substitutions present in their clay layer that induced a more diffuse undersaturation of surface oxygen, compared to saponites. Consistently, Chen et al. (2017) reported only a minor contribution of ammonium heads located above/below Al-substituted tetrahedra from MD simulations performed for a model equivalent to Sap-OH-1.2, although a non-homogeneous distribution of tetrahedral substitutions and initial random location of alkylammonium cations were assumed. The actual location of ammonium heads above Al-substituted tetrahedral or ditrigonal cavities thus appears to result from the balance between local charge compensation and steric hindrance.

Alkyl chains forming the tails of the alkylammonium cations were essentially parallel to the basal surface of the 2:1 layers to optimize steric constraints. Consequently, h1 and h2 configurations essentially correspond to 1 and 2 planes of C atoms from the alkyl chains bound to adjacent layers as initially proposed by Lagaly (1994 – Figs. S4b, S5b). These interlayer configurations were also consistent with the ones reported by Heinz et al. (2007) for stable h1 and h2 configurations computed for C10 and C22 chain lengths (NH₃ head groups) and a CEC 91 meq/100 g (see fig. 1a in Heinz et al., 2007). Finally, MD calculations suggested that the h3 configuration proposed by Lagaly (1994) – Fig. 7, included two major planes of C atoms similar to those observed for the h2 configuration. An intermediate and apparently less organized zone sandwiched in between these two planes hosted sections of the alkyl chains that were not accommodated in the two main planes, similar to the organization of interlayer H₂O molecules in highly hydrated smectites (Dazas et al., 2014).

3.2.2. Stability domains for the different stable configurations

As LLDs calculated from both DFT and classical MD simulations were close to experimentally determined ones, the number of carbon atoms in the alkyl chains corresponding to the experimental transition from one stability domain to another also corresponded nicely to simulation results (Fig. 4). For example, the stability domain of the h1 configuration (apparent LLD within the 12.8–13.7 Å range) extended experimentally from short chain lengths to C10, C7, C5, and C5 for $x = 0.8, 1.0, 1.2,$ and 1.4 , respectively. Similar LLD values (12.8–13.7 Å – Fig. 4) were computed for the h1 configuration from both DFT and classical MD simulations. The decrease of the maximum (critical) chain length allowing this h1 configuration with increasing layer charge density was

consistent with the initial model (Lagaly and Weiss, 1971; Lagaly, 1994). Except for DFT calculations that were performed for $x = 1.5$, these chain lengths corresponded to the maximum alkyl chain length allowing the h1 interlayer configuration in the simulations performed. Similarly, the shortest alkyl chains leading experimentally to the h2 configuration comprised 16, 12, 9, and 9 carbon atoms for $x = 0.8, 1.0, 1.2,$ and 1.4 , respectively (Fig. 4). These chain lengths were consistent with those determined using computational approaches and leading to LLDs typical for the h2 configuration. For MD simulations, the LLD typical of the h2 configuration was slightly higher (18.0–18.7 Å – Fig. 4b) than the distance usually reported experimentally for the h2 configuration. Similar LLDs exceeding 18.0 Å were also reported by Heinz et al. (2007) for the h2 configuration. Compared to the maximum chain length leading experimentally to a stable h2 configuration (18, 15, 11, and 11C atoms for $x = 0.8, 1.0, 1.2,$ and 1.4 , respectively), the stability domain computed for the h2 configuration was extended slightly towards longer alkyl chain lengths (e.g., 16–17C atoms for $x = 1.0$), possibly as the result of the larger LLD computed for this h2 configuration. The stability domain of the h2 configuration computed for lower charge density extended also towards shorter alkyl chain lengths however, as a LLD of 17.7 Å, consistent with this interlayer configuration was computed for $x = 0.8$ and C12 (Fig. 4a).

3.3. Interstratification of different stable configurations and heterogeneity of layer charge density

The extents of the stability domains corresponding to the stable configurations defined by Lagaly and coworkers (Lagaly and Weiss, 1971; Lagaly, 1994) and of the transition zones were essentially similar in both experimental and computational approaches (Fig. 4). LLD evolutions within the transition zones differed strongly in both cases, however. Experimentally determined LLD values increased steadily from those corresponding to one stability domain to the next one, consistent with the random interstratification of different stable interlayer configurations within the same crystals (Méring, 1949; Lanson, 2011 and references therein). This steady evolution is also consistent with the initial definition of the method. XRD data, and more especially the observed broadening of XRD maxima located between these LLDs (Fig. 3) supports such interstratification. Lagaly and coworkers (Lagaly and Weiss, 1971; Lagaly, 1994) related the coexistence of different interlayer configurations within a given crystal to the heterogeneity of layer charge density. The use of synthetic smectites for the experimental section of the present study was expected to reduce significantly this heterogeneity but no specific decrease of the extent of these intermediate domains was observed compared to natural smectites (Lagaly and Weiss, 1970, 1971; Laird et al., 1989; Lagaly, 1994).

Simulation results indicated also the existence of LLDs intermediate between those corresponding to stable configurations (Fig. 4). In contrast to the experimental steady evolution however, computed LLD values usually exhibited a major increase for a small increase of the alkyl chain length typical of the destabilization of one configuration. The rapid LLD evolution possibly results from the lower stability of configurations having LLD values intermediate between those of the stable h1, h2, and h3 configurations. Similarity of experimental and computed transition domains challenges however the original assumption of Lagaly concerning the origin of the interstratification of different interlayer configurations since DFT and MD simulations were systematically performed for homogeneous charge distributions within successive layers and within a given layer. In the present theoretical calculations, the distribution of Al-for-Si substitutions was periodic and thus maximized the homogeneity of layer charge distribution within the layer plane. The mixture (interstratification) of Lagaly's stable configurations is thus likely energetically more favorable than an intermediate configuration to “average” the interlayer space required to compensate for a given layer charge density using a single alkyl chain length.

3.4. Implications for the layer charge determination method using alkylammonium cations

The overall consistency observed in the present study between the stability domains (in terms of alkyl chain length) calculated for h1 and h2 configurations using computational approaches and those determined from XRD data for smectites having well-defined layer-charge deficit confirms the validity of the method that relies mainly on the extent (in terms of alkyl chain length) of these stability domains. The ability of the alkylammonium method to provide layer charge densities consistent with those derived from smectite structural formula was strongly improved however by using the revised equation proposed by Laird et al. (1989). In the present case, layer charge densities deduced from the alkylammonium method and this revised equation were 0.72, 0.99, 1.28, and 1.31 for Sap-OH-x with $x = 0.8, 1.0, 1.2,$ and 1.4 , respectively. Note that layer charge density values obtained using the alkylammonium method may provide a more realistic description of smectite properties, and in particular of their cation exchange capacity however (Kaufhold, 2006; Kaufhold et al., 2011). Adequate corrections to measured cation exchange capacity values may however allow improving the agreement with layer charge densities obtained using the structural formula method (Środoń and McCarty, 2008).

The similar layer charge density values obtained for Sap_OH_1.2 and Sap_OH_1.4 challenge however the ability of the alkylammonium method to accurately determine the layer charge density of high-charge expandable phyllosilicates (vermiculites). For the two samples investigated, the evolution of the position of the first basal reflection as a function of alkyl chain length was typical for low-to-medium charge vermiculites ($x \leq 1.5$ per $O_{20}(OH)_4$), with stepwise, or wave-like, changes of the apparent basal distance with alkyl chain length (Lagaly, 1994). The reduced extension of the domains corresponding to stable h1 and h2 configurations possibly limits the applicability of the routine alkylammonium method. The non-linearity of this evolution allows rejecting also a paraffin-like configuration of alkylammonium cations in these low-to-medium charge vermiculites (Lagaly, 1994). Consistently, the α angle determined from a linear fit to the data ($\text{pos.} = 10.172 + 0.744 \times n, R^2 = 0.9865$) was unrealistically low (36.2°) to allow layer-charge determination using the various empirical curves proposed for high-charge vermiculites (Lagaly and Weiss, 1969; Ghabru et al., 1989; Mermut, 1994). For these low-to-medium charge vermiculites ($1.2 \leq x \leq 1.5$ per $O_{20}(OH)_4$), interstratification of interlayers exhibiting stable h1/h2 configurations and paraffin-like configuration of alkylammonium cations thus appears as a possible alternative hypothesis for the inefficiency of both methods, thus hampering the use of the alkylammonium method for such expandable phyllosilicates. The

stability of paraffin-like configurations for a layer charge $x = 1.5$ (per $O_{20}(OH)_4$) and short alkyl chain lengths (4–5 carbons – Fig. 8) evidenced by DFT calculations supports this hypothesis. The reported modification of interlayer alkylammonium configuration from h1/h2 to paraffin-like with increasing layer charge density may be due to contrasting ordering of isomorphous substitutions in smectites and vermiculites (random and ordered distributions, respectively) or to the contrasting layer charge densities. The alkylammonium method does not hypothesize however on the ordering, or location, of isomorphous substitutions and Dzas et al. (2015) did not evidence any direct relationship between ordering of isomorphous substitutions and that of interlayer cations.

Finally, both DFT and MD simulations showed that even for highly homogeneous layer charge densities, a significant range of carbon chain lengths allowed the presence of LLDs intermediate between those of stable configurations. These intermediate distances correspond experimentally to the interstratification of different stable configurations that were initially thought to be characteristic of layer charge heterogeneity (Lagaly and Weiss, 1971; Lagaly, 1994). Simulations show that intermediate distances, and thus interstratification of different stable configurations, occur also for homogeneous layer charge distributions, thus challenging the ability of the alkylammonium method to describe quantitatively layer charge distributions. Similarity of peak position evolution as a function of alkylammonium chain length determined in the present study from synthetic smectites with those determined from natural smectite of similar layer charge supports this limitation. As a consequence, the benefit expected from the use of the complete series of alkylammonium cations is vanishing. The use of simplified methods using a reduced number of alkyl chain lengths (Olis et al., 1990; Mermut, 1994) is thus to be preferred as their main drawback was supposed to be their inability to provide layer charge distribution (Kaufhold, 2006).

4. Conclusion

Layer-to-layer distances computed from DFT and MD simulations are consistent with those determined experimentally on a series of synthetic saponites with layer charge ranging from medium-charge smectite to medium-charge vermiculite over the whole range of alkyl chain length considered in the present study. Despite minor differences, this consistency confirms the ability of computational methods to accurately predict the organization of large organic molecules in smectite interlayers and to unravel the molecular interactions ruling this organization. DFT simulations allow high-precision predictions of structure models but computational costs do not always allow probing a model with proper stoichiometry. By deriving DFT-optimized models of similar

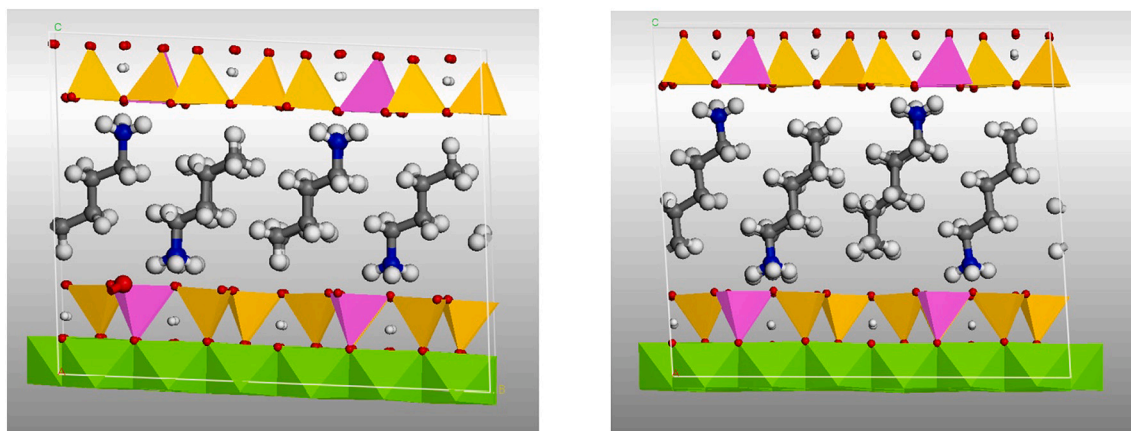


Fig. 8. DFT optimized configuration of saponite interlayer hosting alkylammonium cations in a paraffin-like configuration. Layer charge: $x = 1.5$, alkyl chain length of the interlayer alkylammonium cations: 4 and 5 carbons (left and right, respectively). View along the a axis. Colors as in Fig. 5. Snapshots generated using Materials studio.

stoichiometry, MD simulations allow describing structure models for all possible layer compositions. MD simulations also imply thermalization of the system and allow probing alternative configurations allowed by thermal expansion of DFT-optimized models. For example, location of ammonium heads above/below Al-substituted tetrahedra is not observed in DFT simulations owing to the limited interlayer space, whereas the slight increase of LLD values upon thermalization allows these electrostatically-favored configurations. In addition, although LLD values intermediate between those corresponding to the stable h1, h2, etc. configurations described by Lagaly (1994) may be computed, experimentally determined intermediate distances rather result from the interstratification of different stable configurations, as proposed initially.

The overall consistency of computed and experimental LLD values confirms further the ability of AAM to accurately determine a mean value of layer charge density consistent with smectite structural formula when using the revised equations proposed by Laird et al. (1989). The validity of AAM appears however limited to smectite-group minerals, that is to 2:1 phyllosilicates with layer charge density ranging from ~ 0.5 to ≤ 1.2 per $O_{20}(OH)_4$. For high-charge smectite to medium-charge vermiculites ($1.2 \leq x \leq 1.5$ per $O_{20}(OH)_4$), the coexistence of both stable “layered” and paraffin-like configurations in phyllosilicate interlayers most likely hampers a proper use of the method. Finally, the alkylammonium method is most likely unable to describe quantitatively layer charge distributions even when using the complete series of alkylammonium cations thus questioning the interest of the original method compared to simplified methods involving the use of a reduced number of alkyl chain lengths.

Authors' contributions

BL designed the study and guided all aspects of the work; ML synthesized the saponites and contributed to saponite saturation; MV performed the experiments; NF supervised and contributed to XRD experiments; AB supervised and contributed to the preparation of alkyl ammonium solutions and to saponite saturation; PM performed MD simulations; CPdV performed DFT simulations; BL led the overall discussion and manuscript writing; all co-authors discussed the results and commented on the manuscript.

Declaration of Competing Interest

The authors declare that they have no known competing financial interests or personal relationships that could have influenced the work reported in this article.

Data availability

Data will be made available on request.

Acknowledgments

Part of the simulations presented in this article were performed using the Froggy platform of the GRICAD infrastructure (<https://gricad.univ-grenoble-alpes.fr>), which is supported by the Rhône-Alpes region (GRANT CPER07_13 CIRA) and the Equip@Meso project (reference ANR-10-EQPX-29-01) of the “Investissements d’Avenir” program supervised by the Agence Nationale pour la Recherche. ISTERRE is part of Labex OSUG@2020 (ANR10-LABX56).

Appendix A. Supplementary data

Supplementary data to this article can be found online at <https://doi.org/10.1016/j.clay.2022.106665>.

References

- Aristilde, L., Lanson, B., Charlet, L., 2013. Interstratification patterns from the pH-dependent intercalation of a tetracycline antibiotic within montmorillonite layers. *Langmuir* 29, 4492–4501.
- Bergaoui, L., Lambert, J.-F., Franck, R., Suquet, H., Robert, J.-L., 1995. Al-pillared saponites. Part 3.—effect of parent clay layer charge on the intercalation-pillaring mechanism and structural properties. *J. Chem. Soc. Faraday Trans.* 91, 2229–2239.
- Chen, C., Liu, X., Zhang, Y., Zhang, C., Lu, X., 2017. Molecular dynamics simulation of alkylammonium-intercalated vermiculites. *Clay Clay Miner.* 65, 378–386.
- Christidis, G.E., Blum, A.E., Eberl, D.D., 2006. Influence of layer charge and charge distribution of smectites on the flow behaviour and swelling of bentonites. *Appl. Clay Sci.* 34, 125–138.
- Cicel, B., Komadel, P., 1994. Structural formulae of layer silicates. In: Amonette, J.E., Zelazny, L.W. (Eds.), *Quantitative Methods in Soil Mineralogy*. Soil Science Society of America, Madison, Wisconsin, USA, pp. 114–136.
- Corbin, G., Vulliet, E., Lanson, B., Rimola, A., Mignon, P., 2021. Adsorption of pharmaceuticals onto smectite clay minerals: a combined experimental and theoretical study. *Minerals* 11, 62.
- Cygan, R.T., Liang, J.-J., Kalinichev, A.G., 2004. Molecular models of hydroxide, oxyhydroxide, and clay phases and the development of a general force field. *J. Phys. Chem. B* 108, 1255–1266.
- Dazas, B., Ferrage, E., Delville, A., Lanson, B., 2014. Interlayer structure model of tri-hydrated low-charge smectite by X-ray diffraction and Monte Carlo modeling in the Grand Canonical ensemble. *Am. Mineral.* 99, 1724–1735.
- Dazas, B., Lanson, B., Delville, A., Robert, J.-L., Komarneni, S., Michot, L.J., Ferrage, E., 2015. Influence of tetrahedral layer charge on the organization of interlayer water and ions in synthetic Na-saturated smectites. *J. Phys. Chem. C* 119, 4158–4172.
- Dohrmann, R., 2006. Cation exchange capacity methodology I: an efficient model for the detection of incorrect cation exchange capacity and exchangeable cation results. *Appl. Clay Sci.* 34, 31–37.
- Dohrmann, R., Kaufhold, S., Echle, W., Meyer, F.M., 1999. Beyond the Methylene Blue Test: Introduction of the cu(II)-Triethylene Tetramine Method for Smectite Estimation in Bentonite, Euroclay, Krakow, Poland, p. 76.
- Feng, Y., Williams, G.R., Leroux, F., Taviot-Guého, C., O’Hare, D., 2006. Selective anion-exchange properties of second-stage layered double hydroxide heterostructures. *Chem. Mater.* 18, 4312–4318.
- Ferrage, E., 2016. Investigation of the interlayer organization of water and ions in smectite from the combined use of diffraction experiments and molecular simulations: a review of methodology, applications, and perspectives. *Clay Clay Miner.* 64, 348–373.
- Ferrage, E., Lanson, B., Sakharov, B.A., Drits, V.A., 2005. Investigation of smectite hydration properties by modeling experimental X-ray diffraction patterns: part I. Montmorillonite hydration properties. *Am. Mineral.* 90, 1358–1374.
- Ferrage, E., Lanson, B., Sakharov, B.A., Geoffroy, N., Jacquot, E., Drits, V.A., 2007. Investigation of dioctahedral smectite hydration properties by modeling of X-ray diffraction profiles: influence of layer charge and charge location. *Am. Mineral.* 92, 1731–1743.
- Ferrage, E., Lanson, B., Michot, L.J., Robert, J.L., 2010. Hydration properties and interlayer organization of water and ions in synthetic Na-smectite with tetrahedral layer charge. Part 1. Results from X-ray diffraction profile modeling. *J. Phys. Chem. C* 114, 4515–4526.
- Ferrage, E., Sakharov, B.A., Michot, L.J., Delville, A., Bauer, A., Lanson, B., Grangeon, S., Frapper, G., Jimenez-Ruiz, M., Cuello, G.J., 2011. Hydration properties and interlayer organization of water and ions in synthetic Na-smectite with tetrahedral layer charge. Part 2. Towards a precise coupling between molecular simulations and diffraction data. *J. Phys. Chem. C* 115, 1867–1881.
- Gates, W.P., Bouazza, A., Churchman, G.J., 2009. Bentonite clay keeps pollutants at bay. *Elements* 5, 105–110.
- Ghabru, S.K., Mermut, A.R., Arnaud, R.J.S., 1989. Layer-charge and cation-exchange characteristics of vermiculite (Weathered biotite) isolated from a gray lusivol in northeastern Saskatchewan. *Clay Clay Miner.* 37, 164–172.
- Glaeser, R., Méring, J., 1954. Isothermes d’hydratation des montmorillonites bi-ioniques (Ca, Na). *Clay Miner. Bull.* 2, 188–193.
- Guggenheim, S., Adams, J.M., Bain, D.C., Bergaya, F., Brigatti, M.F., Drits, V.A., Formoso, M.L.L., Galan, E., Kogure, T., Stanjek, H., 2006. Summary of recommendations of nomenclature committees relevant to clay mineralogy: report of the Association Internationale pour l’Etude des Argiles (AIPEA) Nomenclature Committee for 2006. *Clay Miner.* 41, 863–877.
- Hamilton, D.L., Henderson, C.M.B., 1968. The preparation of silicate compositions by a gelling method. *Miner. Mag.* 36, 832–838.
- Heinz, H., Vaia, R.A., Krishnamoorti, R., Farmer, B.L., 2007. Self-assembly of alkylammonium chains on montmorillonite: effect of chain length, head group structure, and cation exchange capacity. *Chem. Mater.* 19, 59–68.
- Hernández-Haro, N., Muñoz-Santiburcio, D., Del Valle, C.P., Ortega-Castro, J., Sainz-Díaz, C.I., Garrido, C.J., Hernández-Laguna, A., 2016. Compressibility of 2M₁ muscovite-paragonite series minerals: a computational study to 6 GPa. *Am. Mineral.* 101, 1207–1216.
- Hobza, P., Kabeláč, M., Šponer, J., Mejzlík, P., Vondrášek, J., 1997. Performance of empirical potentials (AMBER, CFF95, CVFF, CHARMM, OPLS, POLTEV), semiempirical quantum chemical methods (AMI, MNDO/M, PM3), and ab initio Hartree-Fock method for interaction of DNA bases: Comparison with nonempirical beyond Hartree-Fock results. *J. Comput. Chem.* 18, 1136–1150.
- Jackson, M.L., 2005. *Soil Chemical Analysis - Advanced Course, Revision of 2nd Edition* - 11th printing ed. Parallel Press, Univ. Wisconsin-Madison Libraries, Madison, WI.

- Kaufhold, S., 2006. Comparison of methods for the determination of the layer charge density (LCD) of montmorillonites. *Appl. Clay Sci.* 34, 14–21.
- Kaufhold, S., Dohrmann, R., Stucki, J.W., Anastácio, A.S., 2011. Layer charge density of smectites - closing the gap between the structural formula method and the alkyl ammonium method. *Clay Clay Miner.* 59, 200–211.
- Lagaly, G., 1981. Characterization of clays by organic compounds. *Clay Miner.* 16, 1–21.
- Lagaly, G., 1994. Layer charge determination by alkylammonium ions. In: Mermut, A.R. (Ed.), *Layer Charge Characteristics of 2:1 Silicate Clay Minerals*. Clay Minerals Society, Aurora, CO, pp. 1–46.
- Lagaly, G., Weiss, A., 1969. Determination of the layer charge in mica type layer silicates. In: Heller, L. (Ed.), *International Clay Conference*. Israel University Press, Jerusalem, Tokyo, Japan, pp. 61–80.
- Lagaly, G., Weiss, A., 1970. Anordnung und Orientierung kationischer Tenside auf Silicatoberflächen. *Kolloid-Z. u. Z. Polymere* 238, 485–493.
- Lagaly, G., Weiss, A., 1971. Anordnung und Orientierung kationischer Tenside auf Silicatoberflächen. *Kolloid-Z. u. Z. Polymere* 243, 48–55.
- Laird, D.A., 1994. Evaluation of structural formulae and alkylammonium methods of determining layer charge. In: Mermut, A.R. (Ed.), *Layer Charge Characteristics of 2:1 Silicate Clay Minerals*. Clay Minerals Society, Chantilly, VA, pp. 79–104.
- Laird, D.A., 2006. Influence of layer charge on swelling of smectites. *Appl. Clay Sci.* 34, 74–87.
- Laird, D.A., Scott, A.D., Fenton, T.E., 1989. Evaluation of the alkylammonium method of determining layer charge. *Clay Clay Miner.* 37, 41–46.
- Lanson, B., 2011. Modelling of X-ray diffraction profiles: Investigation of defective lamellar structure crystal chemistry. In: Brigatti, M.F., Mottana, A. (Eds.), *Layered Mineral Structures and their Application in Advanced Technologies*. Mineralogical Society Great Britain & Ireland, London, pp. 151–202.
- Liu, X., Lu, X., Wang, R., Zhou, H., Xu, S., 2007. Interlayer structure and dynamics of alkylammonium-intercalated smectites with and without water: a molecular dynamics study. *Clay Clay Miner.* 55, 554–564.
- Méring, J., 1949. L'interférence des rayons-X dans les systèmes à stratification désordonnée. *Acta Crystallogr.* 2, 371–377.
- Méring, J., Glaeser, R., 1954. Sur le rôle de la valence des cations échangeables dans la montmorillonite. *Bull. Soc. Fr. Minér. Cristallogr.* 77, 519–530.
- Mermut, A.R., 1994. Problems associated with layer charge characterization of phyllosilicates. In: Mermut, A.R. (Ed.), *Layer Charge Characteristics of 2:1 Silicate Clay Minerals*. Clay Minerals Society, Chantilly, VA, pp. 106–122.
- Michot, L.J., Villieras, F., 2002. Assessment of surface energetic heterogeneity of synthetic Na-saponites. The role of layer charge. *Clay Miner.* 37, 39–57.
- Mignon, P., Corbin, G., Le Crom, S., Marry, V., Hao, J., Daniel, L., 2020. Adsorption of nucleotides on clay surfaces: effects of mineral composition, pH and solution salts. *Appl. Clay Sci.* 190, 105544.
- Möller, M.W., Hirsemann, D., Haarmann, F., Senker, J., Breu, J., 2010. Facile scalable synthesis of rectorites. *Chem. Mater.* 22, 186–196.
- Moore, D.M., Reynolds Jr., R.C., 1997. *X-Ray Diffraction and the Identification and Analysis of Clay Minerals*. Oxford University Press, Oxford.
- Newman, A.C.D., Brown, G., 1987. The chemical constitution of clays. In: Newman, A.C. D. (Ed.), *Chemistry of Clays and Clay Minerals*. John Wiley and Sons, New York, NY, USA, pp. 1–128.
- Olis, A.C., Malla, P.B., Douglas, L.A., 1990. The rapid estimation of the layer charges of 2:1 expanding clays from a single alkylammonium ion expansion. *Clay Miner.* 25, 39–50.
- Paineau, E., Bihannic, I., Baravian, C., Philippe, A.-M., Davidson, P., Levitz, P., Funari, S. S., Rochas, C., Michot, L.J., 2011a. Aqueous suspensions of natural swelling clay minerals. 1. Structure and electrostatic interactions. *Langmuir* 27, 5562–5573.
- Paineau, E., Michot, L.J., Bihannic, I., Baravian, C., 2011b. Aqueous suspensions of natural swelling clay minerals. 2. Rheological characterization. *Langmuir* 27, 7806–7819.
- Plimpton, S., 1995. Fast parallel algorithms for short-range molecular dynamics. *J. Comput. Phys.* 117, 1–19.
- Robert, J.L., Beny, J.M., Della Ventura, G., Hardy, M., 1993. Fluorine in micas: crystal-chemical control of the OH-F distribution between trioctahedral and dioctahedral sites. *Eur. J. Mineral.* 5, 7–18.
- Sanz, J., Robert, J.-L., 1992. Influence of structural factors on ^{29}Si and ^{27}Al NMR chemical shifts of phyllosilicates 2:1. *Phys. Chem. Miner.* 19, 39–45.
- Sanz, J., Robert, J.-L., Diaz, M., Sobrados, I., 2006. Influence of charge location on ^{29}Si NMR chemical shift of 2:1 phyllosilicates. *Am. Mineral.* 91, 544–550.
- Sato, T., Watanabe, T., Otsuka, R., 1992. Effects of layer charge, charge location, and energy change on expansion properties of dioctahedral smectites. *Clay Clay Miner.* 40, 103–113.
- Soler, J.M., Artacho, E., Gale, J.D., García, A., Junquera, J., Ordejón, P., Sánchez-Portal, D., 2002. The SIESTA method for ab initio order-N materials simulation. *J. Phys. Condens. Matter* 14, 2745–2779.
- Środoń, J., McCarty, D.K., 2008. Surface area and layer charge of smectite from CEC and EGME/H₂O-retention measurements. *Clay Clay Miner.* 56, 155–174.
- Stanjek, H., Friedrich, R., 1986. The determination of layer charge by curve-fitting of Lorentz- and polarization-corrected X-ray diagrams. *Clay Miner.* 21, 183–190.
- Stanjek, H., Niederbudde, E.A., Hausler, W., 1992. Improved evaluation of layer charge of n-alkylammonium-treated fine soil clays by Lorentz- and polarization-correction and curve-fitting. *Clay Miner.* 27, 3–19.
- Swadling, J.B., Coveney, P.V., Greenwell, H.C., 2010. Clay minerals mediate folding and regioselective interactions of RNA: a large-scale atomistic simulation study. *J. Am. Chem. Soc.* 132, 13750–13764.
- Swadling, J.B., Suter, J.L., Greenwell, H.C., Coveney, P.V., 2013. Influence of surface chemistry and charge on mineral-RNA interactions. *Langmuir* 29, 1573–1583.
- Szczerba, M., Kalinichev, A.G., 2016. Intercalation of ethylene glycol in smectites: several molecular simulation models verified by X-ray diffraction data. *Clay Clay Miner.* 64, 488–502.
- Szczerba, M., Klapka, Z., Kalinichev, A., 2014. Ethylene glycol intercalation in smectites. Molecular dynamics simulation studies. *Appl. Clay Sci.* 91–92, 87–97.
- Taviot-Guého, C., Feng, Y., Faour, A., Leroux, F., 2010. Intercalation chemistry in a LDH system: anion exchange process and staging phenomenon investigated by means of time-resolved, *in situ* X-ray diffraction. *Dalton Trans.* 39, 5994–6005.
- Thyveetil, M.-A., Coveney, P.V., Greenwell, H.C., Suter, J.L., 2008. Computer simulation study of the structural stability and materials properties of DNA-intercalated layered double hydroxides. *J. Am. Chem. Soc.* 130, 4742–4756.
- Troullier, N., Martins, J.L., 1991. Efficient pseudopotentials for plane-wave calculations. II. Operators for fast iterative diagonalization. *Phys. Rev. B* 43, 8861–8869.
- Vaia, R.A., Teukolsky, R.K., Giannelis, E.P., 1994. Interlayer structure and molecular environment of alkylammonium layered silicates. *Chem. Mater.* 6, 1017–1022.
- Vinci, D., Dazas, B., Ferrage, E., Lanson, M., Magnin, V., Findling, N., Lanson, B., 2020. Influence of layer charge on hydration properties of synthetic octahedrally-charged Na-saturated trioctahedral swelling phyllosilicates. *Appl. Clay Sci.* 184, 105404.
- Wang, J., Wolf, R.M., Caldwell, J.W., Kollman, P.A., Case, D.A., 2004. Development and testing of a general Amber force field. *J. Comput. Chem.* 25, 1157–1174.
- Woods, R.J., Chappelle, R., 2000. Restrained electrostatic potential atomic partial charges for condensed-phase simulations of carbohydrates. *J. Mol. Struct. THEOCHEM* 527, 149–156.
- Young, M.A., Jayaram, B., Beveridge, D.L., 1997. Intrusion of counterions into the spine of hydration in the minor groove of B-DNA: fractional occupancy of electronegative pockets. *J. Am. Chem. Soc.* 119, 59–69.

1 **Determination of layer charge density in expandable phyllosilicates with alkylammonium ions:**
2 **A combined experimental and theoretical assessment of the method**

3
4 Bruno Lanson^{a,*}, Pierre Mignon^b, Mélusine Velde^{a,c,d}, Andreas Bauer^c,
5 Martine Lanson^a, Nathaniel Findling^a, Carlos Perez del Valle^e

6
7
8 Supplementary information

9
10
11 ^aUniv. Grenoble Alpes, Univ. Savoie Mont Blanc, CNRS, IRD, Univ. Gustave Eiffel, ISTERre, F-
12 38000 Grenoble, France

13 ^bUniv. Lyon, Univ. Claude Bernard Lyon 1, CNRS, Institut Lumière Matière, F-69622,
14 Villeurbanne, France

15 ^cFriedrich-Schiller-University Jena (FSU), Institute of Geosciences, Applied Geology, Burgweg
16 11, 07749, Jena, Germany

17 ^dDepartment of Biological Sciences, University of Chicago, USA

18 ^eUniv. Grenoble Alpes, CNRS, DCM, F-38000 Grenoble, France

19
20 * Corresponding author: bruno.lanson@univ-grenoble-alpes.fr

21

22 **Table S1** Alkylamines used for the preparation of alkyl chains

Alkyl chain name	Chain length	CAS number
propylamine	3	107-10-8
butylamine	4	109-73-9
amylamine (pentylamine)	5	110-58-7
hexylamine	6	111-26-2
heptylamine	7	111-68-2
octylamine	8	111-86-4
nonylamine	9	112-20-9
decylamine	10	2016-57-1
undecylamine	11	7307-55-3
dodecylamine	12	124-22-1
tridecylamine	13	2869-34-3
tetradecylamine	14	2016-42-4
pentadecylamine	15	2570-26-5
hexadecylamine	16	143-27-1
heptadecylamine	17	-
octadecylamine	18	124-30-1

24 **Table S2** Amounts of the different chemicals used for the preparation of alkyl chains [modified and extended from Lagaly (1994)].

Length of the alkylamine chain	Mass of alkylamine (g)	Approx. volume of HCl to neutralize the solution (mL)	[HCl] used to neutralize the solution (mol/L)	Approx. Vol. of additional ethanol (mL)	Expected alkylamine final concentration (mol/L)
3	118.2	130	10.27		2.0
4	146.3	185	10.27		2.0
5	174.3	200	10.27		2.0
6	202.4	210	10.27		2.0
7	57.6	250	2		0.5
8	64.6	260	2		0.5
9	71.6	250	2		0.5
10	78.6	250	2		0.5
11	17.1	52	2		0.1
12	18.5	60	2		0.1
13	19.9		2		0.1
14	21.3	50	2	112	0.1
15	22.7	50	2	100	0.1
16	12.1	20	2	250	0.05
17	-	-	-	-	-
18	13.5	25	2	350	0.05

25

26

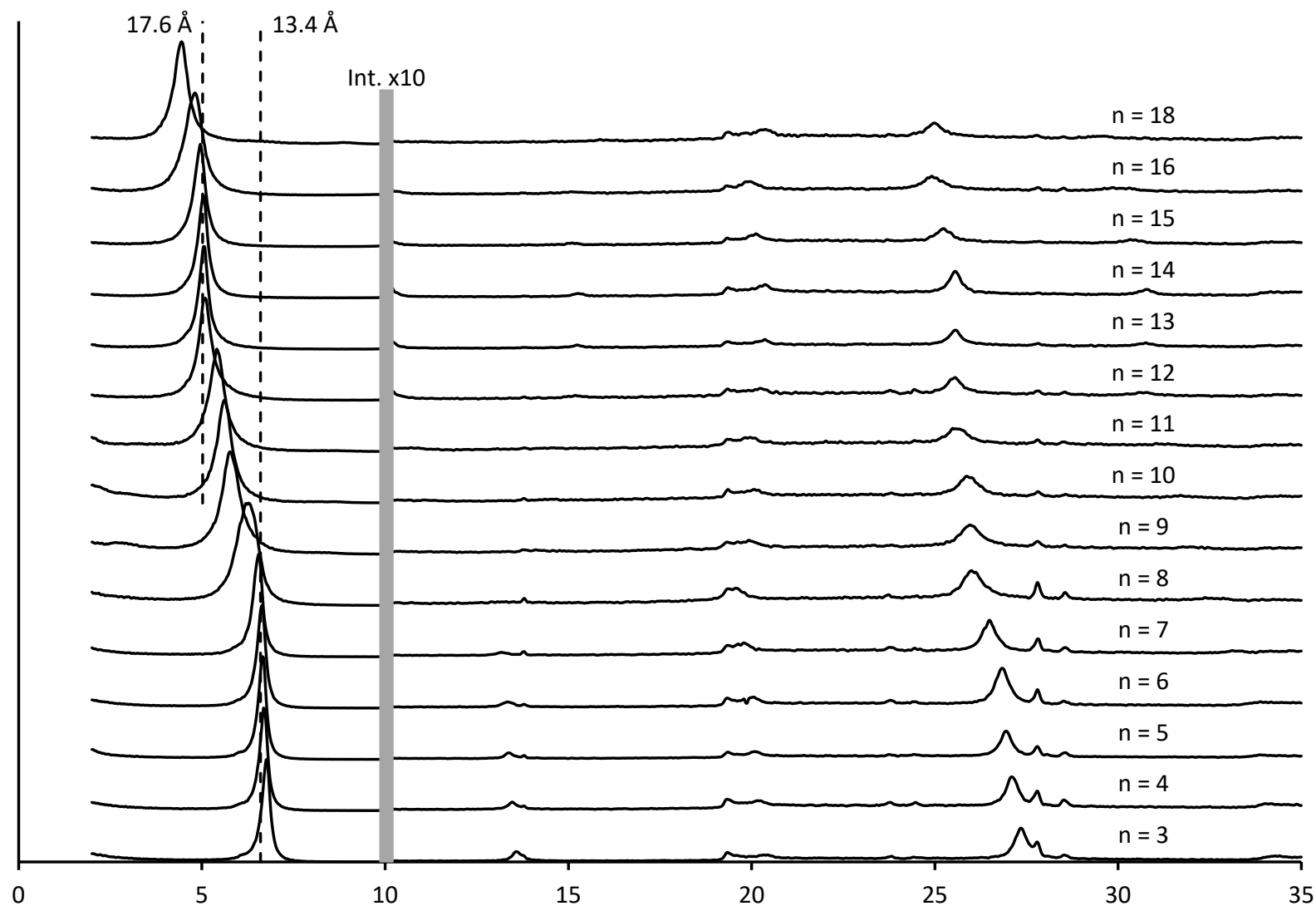
27 **TABLE S3** Details of the atomic models used for molecular dynamics simulations. Number of tetrahedral substitutions (Nb sub) in the 6a × 4b
28 super-cell used for the simulations, and resulting layer charge deficit.

29

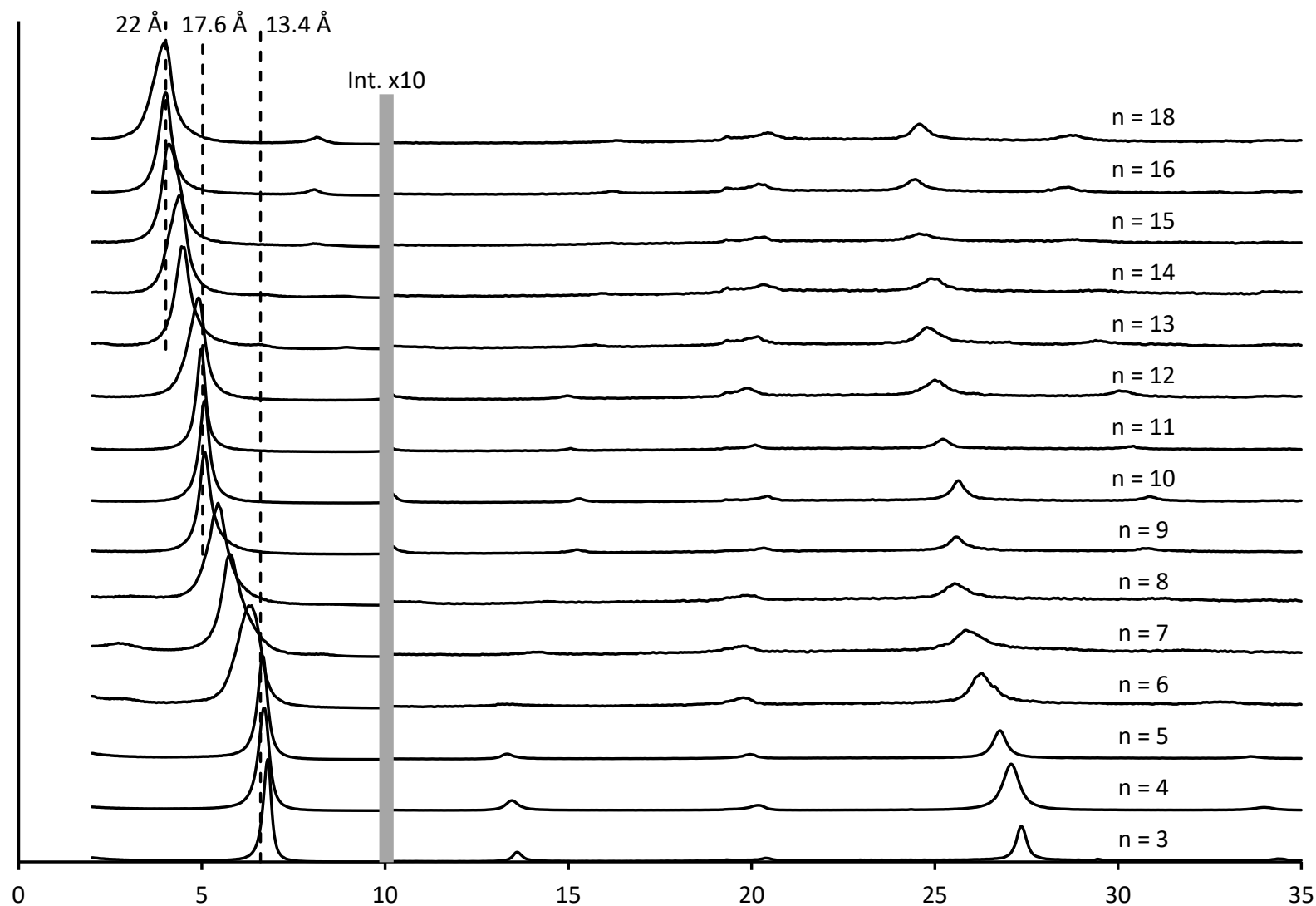
	x=0.8	x=1.0	x=1.2	x=1.4
Nb Sub	18	24	28	34
charge	0.75	1.00	1.17	1.42

30

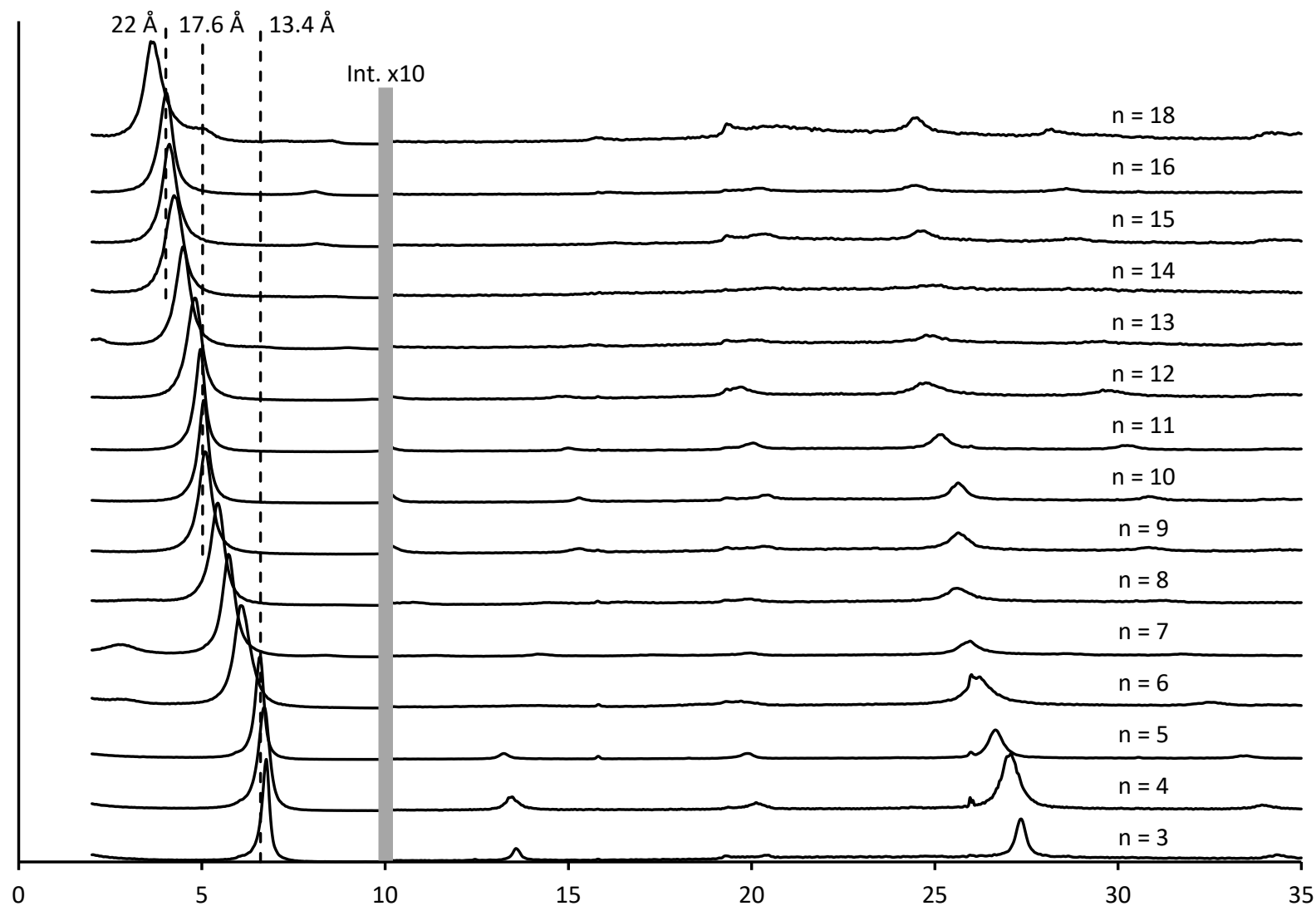
31 **Fig. S1.** X-ray diffraction patterns recorded on Sap-OH-1.0 as a function of the alkyl chain length of the interlayer alkylammonium cation (expressed
32 as the number n of carbon atoms in the alkyl chain). Data were collected at 5 %RH. Dashed lines indicate the layer-to-layer distances typical for
33 monolayers and bilayers of interlayer alkylammonium cations [h1 and h2 configurations of Lagaly (1994), respectively].



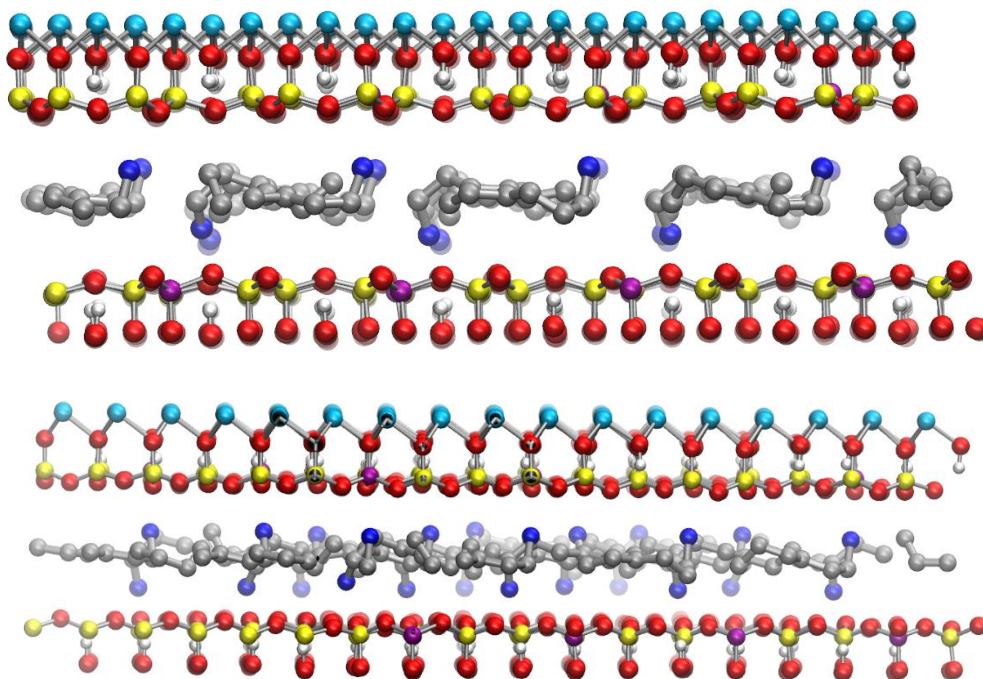
35 **Fig. S2.** X-ray diffraction patterns recorded on Sap-OH-1.2 as a function of the alkyl chain length of the interlayer alkylammonium cation (expressed
36 as the number n of carbon atoms in the alkyl chain). Data were collected at 5 %RH. Dashed lines indicate the layer-to-layer distances typical for
37 mono-, bi- and pseudo tri-layers of interlayer alkylammonium cations [h1, h2, and h3 configurations of Lagaly (1994), respectively].



39 **Fig. S3.** X-ray diffraction patterns recorded on Sap-OH-1.4 as a function of the alkyl chain length of the interlayer alkylammonium cation (expressed
40 as the number n of carbon atoms in the alkyl chain). Data were collected at 5 %RH. Dashed lines indicate the layer-to-layer distances typical for
41 mono-, bi- and pseudo tri-layers of interlayer alkylammonium cations [h1, h2, and h3 configurations of Lagaly (1994), respectively].



43 **Fig. S4a** Representative MD snapshots of alkylammonium saponite hosting a single plane of
44 interlayer alkylammonium cations [h1 configuration from Lagaly (1994)]. Layer charge: $x = 1.0$, alkyl
45 chain length of the interlayer alkylammonium cation: 6 carbons. From top to bottom, views along a
46 and b axes, respectively. Si, Al, Mg, O, N, C, and H atoms are shown as yellow, magenta, light blue,
47 dark blue, dark grey, and white balls, respectively. H atoms from the alkylammonium cations are
48 not shown.

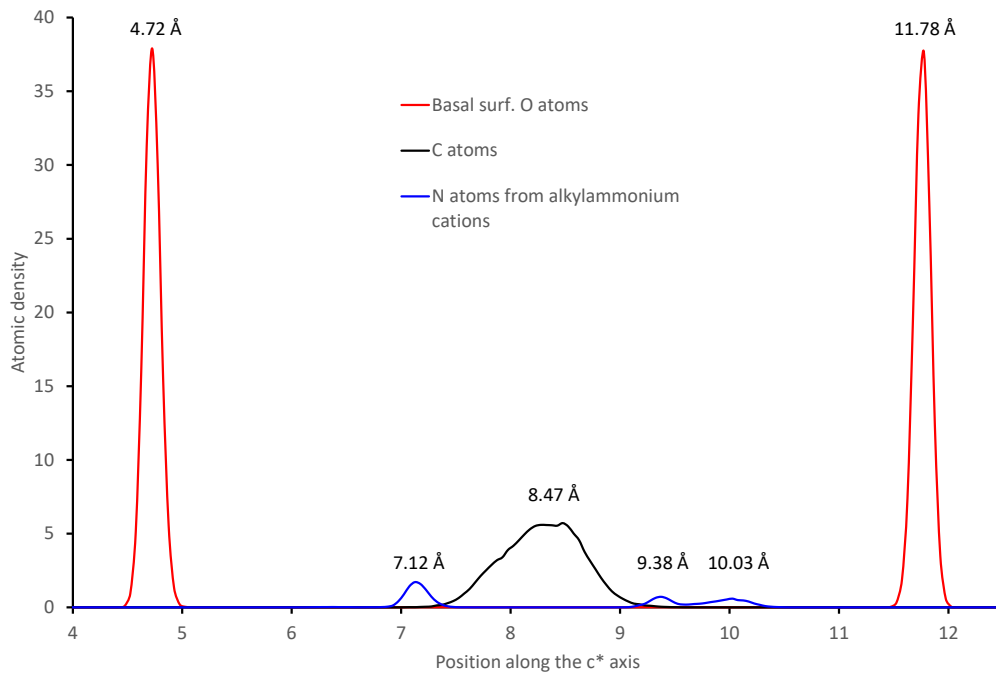


49

50

51

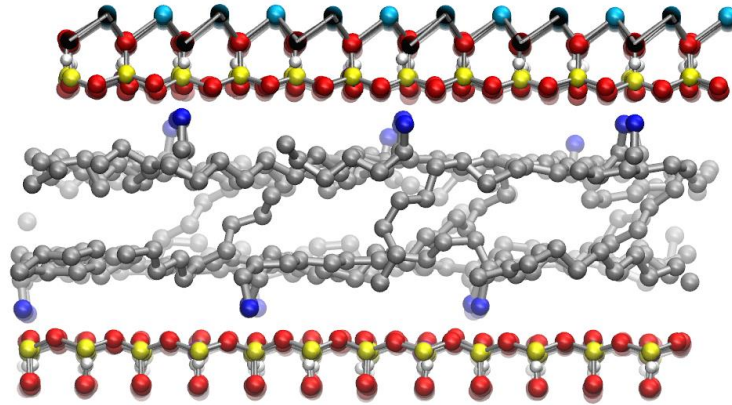
52 **Fig. S4b** Distribution of atomic density derived from MD calculations for alkylammonium saponite
53 hosting a single plane of interlayer alkylammonium cations [h1 configuration from Lagaly (1994)] in
54 projection along the c^* axis. Layer charge: $x = 0.8$, alkyl chain length : 6 carbons. Solid red, black, and
55 blue lines represent O atoms from the 2:1 layer surface and C and N atoms from the interlayer
56 alkylammonium cation, respectively.



57

58

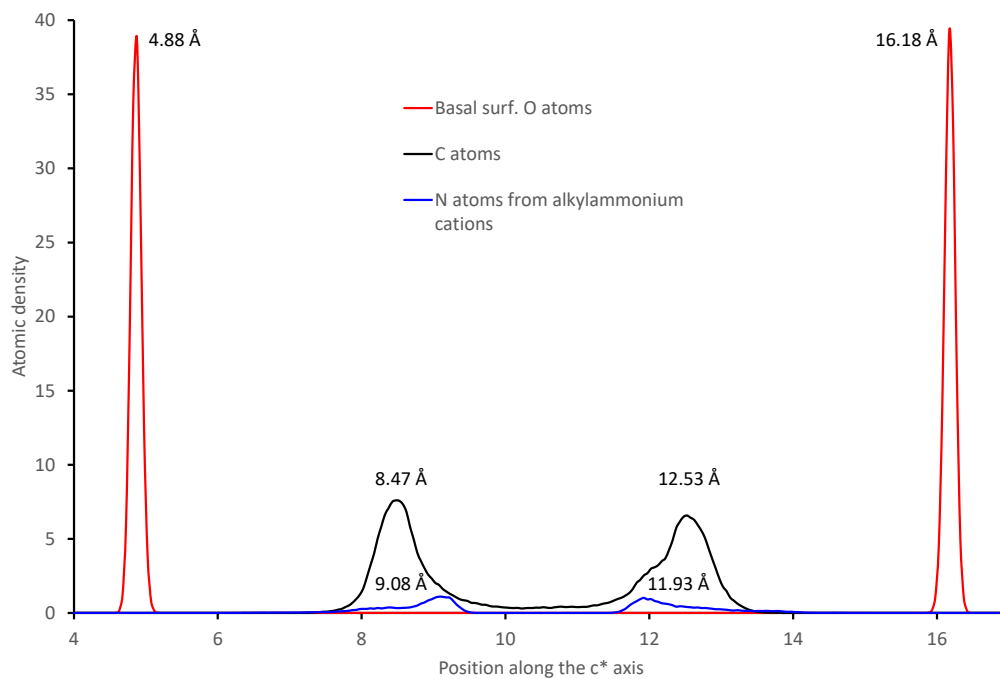
59 **Fig. S5a** Representative MD snapshots of alkylammonium saponite hosting two planes of interlayer
60 alkylammonium cations [h2 configuration from Lagaly (1994)]. Layer charge: $x = 1.0$, alkyl chain
61 length of the interlayer alkylammonium cation: 14 carbons. View along the b axis. Colors as in Fig.
62 S4a.



63

64

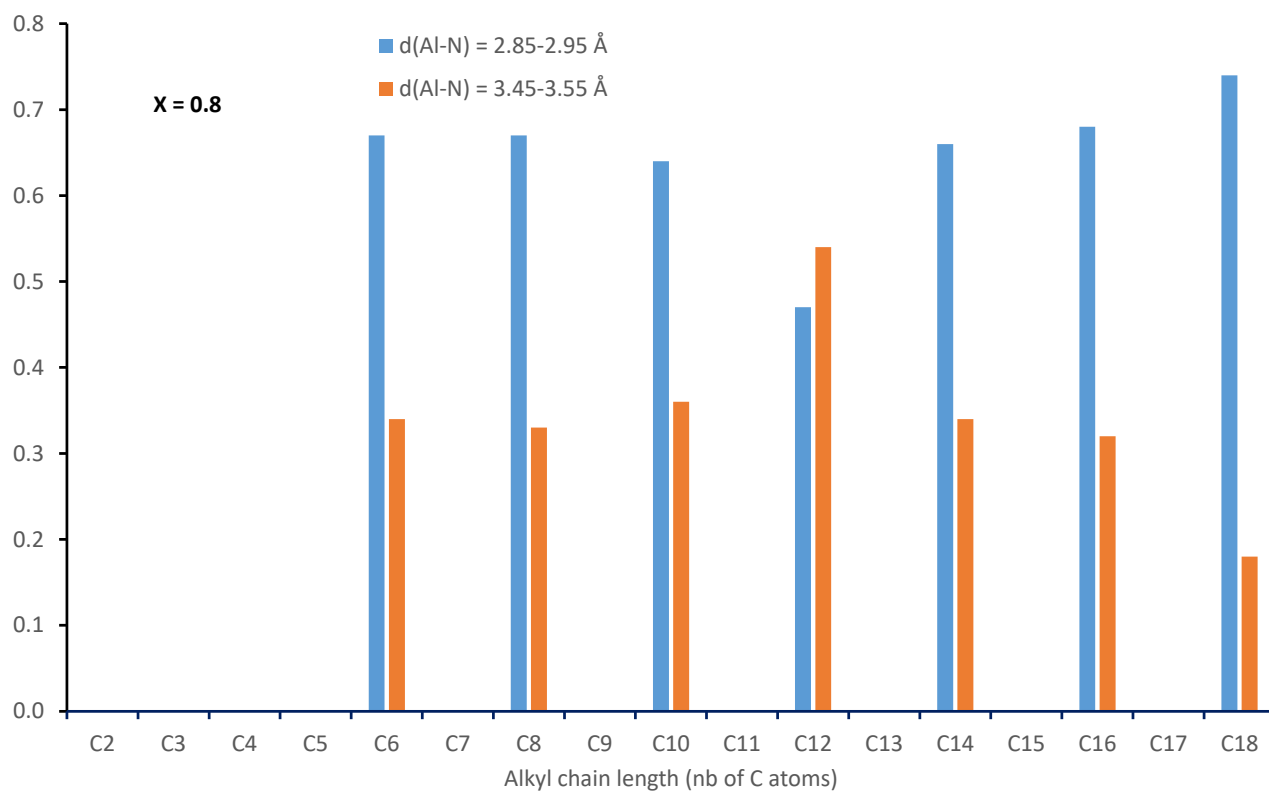
65 **Fig. S5b** Distribution of atomic density derived from MD calculations for alkylammonium saponite
66 hosting two planes of interlayer alkylammonium cations [h2 configuration from Lagaly (1994)] in
67 projection along the c^* axis. Layer charge: $x = 0.8$, alkyl chain length: 14 carbons. Solid red, black,
68 and blue lines represent O atoms from the 2:1 layer surface and C and N atoms from the interlayer
69 alkylammonium cation, respectively.



70

71

72 **Fig. S6** Relative proportions of ammonium heads located above Al-substituted tetrahedra and ditrigonal
73 cavities (blue and orange, respectively) determined from molecular dynamics simulations for different alkyl
74 chain lengths ($x = 0.8$).



75

76

77 **References**

- 78 Lagaly, G., 1994. Layer charge determination by alkylammonium ions, in: Mermut, A.R. (Ed.), Layer charge
79 characteristics of 2:1 silicate clay minerals. Clay Minerals Society, Aurora, Co, pp. 1-46.